TICAM REPORT 98-15
July, 1998

Finite Element Approximations to the System of Shallow Water Equations, Part III: On the Treatment of Boundary Conditions

Clinton N. Dawson and Monica L. Martinez-Canales

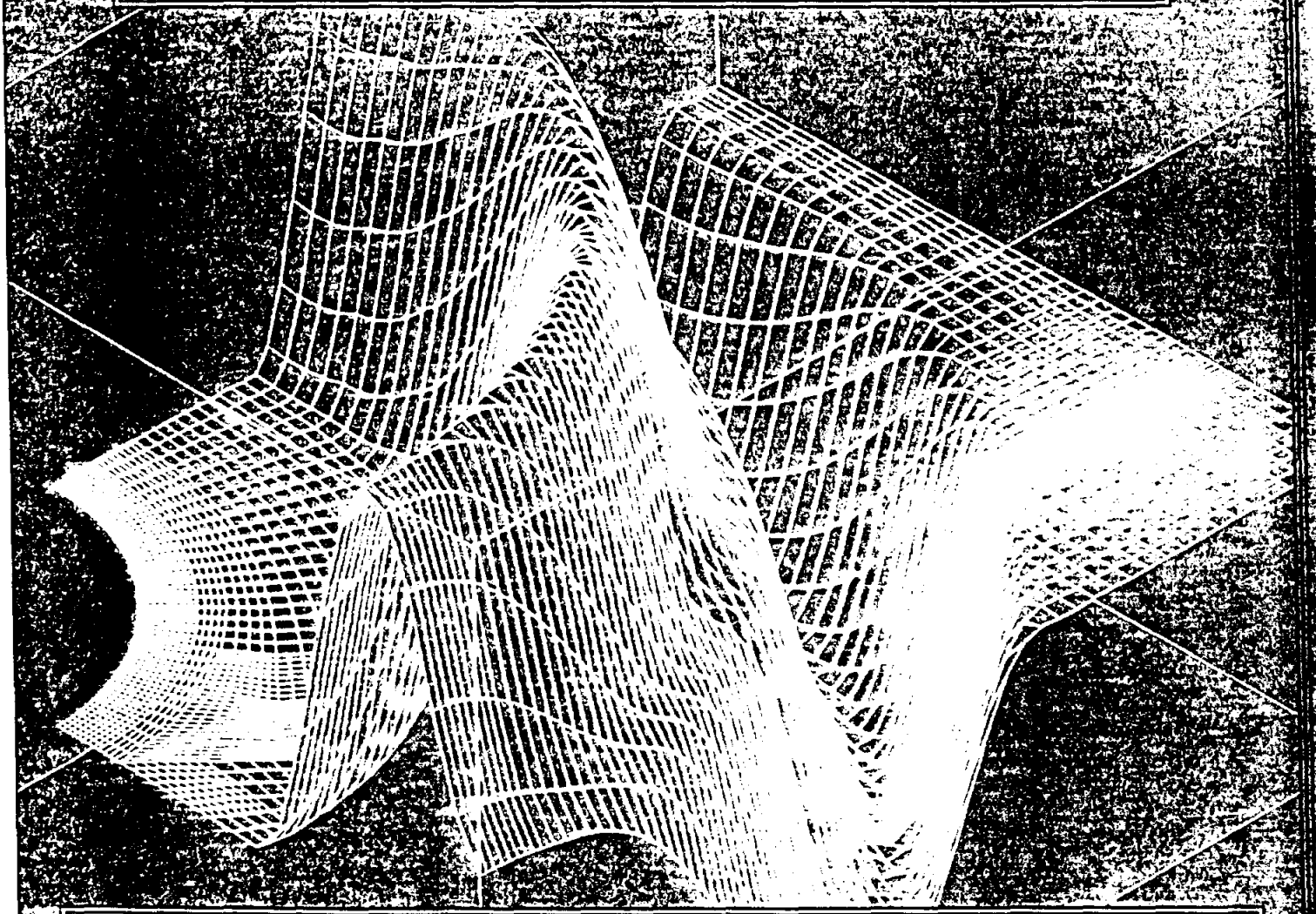

TEXAS INSTITUTE FOR COMPUTATIONAL AND APPLIED MATHEMATICS
THE UNIVERSITY OF TEXAS AT AUSTIN

FINITE ELEMENT APPROXIMATIONS TO THE SYSTEM OF SHALLOW WATER EQUATIONS, PART III: ON THE TREATMENT OF BOUNDARY CONDITIONS *

CLINT N. DAWSON† AND MÓNICA L. MARTÍNEZ-CANALES‡

Abstract. We continue our investigation of finite element approximations to the system of shallow water equations, based on the generalized wave continuity equation (GWCE) formulation. In previous work, we analyzed this system assuming Dirichlet boundary conditions on both elevation and velocity. Based on physical grounds, it is possible to not impose boundary conditions on elevation. Thus, we examine the formulation for the case of Dirichlet conditions on velocity only. The changes required to the finite element method are presented, and stability and error estimates are derived for both an approximate linear model and a full nonlinear model, assuming continuous time. Stability for a discrete time method is also shown.

Key words. boundary conditions, shallow water equations, wave shallow water equations, error estimates

AMS subject classifications. 35Q35, 35L65 65N30, 65N15

1. Introduction. In this paper, we continue our investigation of finite element methods applied to the GWCE (Generalized Wave Continuity Equation) shallow water model of Gray *et al.* This model is described in a series of papers beginning in [8]. It has served as the basis for many shallow water simulators, most notably the Advanced Circulation Model (ADCIRC) described, for example, in [7]. The method has the advantages that it allows for a weaker coupling between the continuity and momentum equations, gives rise to symmetric positive definite matrices, and helps stabilize the numerical solution. These have been supported by a large number of studies (see [5, 6] and references therein).

In previous papers [3, 4], we derived *a priori* error estimates for the method, in both continuous and discrete time, assuming Dirichlet boundary conditions on both the free surface elevation and velocity. In this paper, we will relax this assumption on the elevation and discuss the changes to the model and to the analysis. As it turns out, the assumption of Dirichlet boundary conditions on elevation allowed for a crucial substitution which substantially simplified the analysis. However, by making appropriate changes to the model, we will demonstrate that we are still able to preserve the accuracy of the method, at the cost of some additional computational work.

We will denote by $\xi(\boldsymbol{x},t)$ the free surface elevation over a reference plane and by $h_b(\boldsymbol{x})$ the bathymetric depth under that reference plane so that $H(\boldsymbol{x},t) = \xi + h_b$ is the total water column. Also, we denote by $\boldsymbol{u} = [u(\boldsymbol{x},t)\ v(\boldsymbol{x},t)]^T$ the depth-averaged horizontal velocities and we let $\boldsymbol{U} = \boldsymbol{u}H$.

We will start with the following simplified linear shallow water model:

$$\xi_t + \nabla \cdot \boldsymbol{U} = 0, \tag{1}$$

$$\boldsymbol{U}_t + G\nabla\xi - \mu\Delta\boldsymbol{U} = \boldsymbol{\mathcal{F}}, \tag{2}$$

*This work was supported in part by National Science Foundation, Project No. DMS-9408151.

†Center for Subsurface Modeling - C0200; Texas Institute for Computational and Applied Mathematics; The University of Texas at Austin; Austin, TX 78712.

‡Dept. of Geological and Environmental Sciences; Braun Hall, Bldg 320; Stanford University; Stanford, CA 94305-2115.

which we solve over a domain $\Omega \times (0,T]$. Here $G > 0$ is a gravitational constant and $\mu > 0$ is the eddy viscosity coefficient.

Note that, integrating (1) over Ω,

$$\int_\Omega \xi_t d\Omega + \int_{\partial\Omega} \boldsymbol{U} \cdot \nu ds = 0,$$

where ν is the outward normal to $\partial\Omega$. Moreover, integrating (2) over Ω,

$$\int_\Omega [\boldsymbol{U}_t + G\nabla\xi]\, d\Omega - \mu \int_{\partial\Omega} \nabla \boldsymbol{U} \cdot \nu ds = \int_\Omega \mathcal{F} d\Omega.$$

Thus, it is necessary to specify some type of Dirichlet or Neumann boundary condition on $\boldsymbol{U}$, but it is not required (nor may it be desirable) to specify a boundary condition on ξ.

We will assume the Dirichlet boundary condition

$$\boldsymbol{U} = \boldsymbol{g}, \tag{3}$$

on $\partial\Omega \times (0,T]$. We also assume initial conditions

$$\xi(x,0) = \xi^0(x), \quad \boldsymbol{U}(x,0) = \boldsymbol{U}^0(x). \tag{4}$$

The GWCE is obtained by differentiating (1) with respect to time and substituting the divergence of (2) into the result. We then obtain

$$\xi_{tt} - \nabla \cdot (G\nabla\xi) + \mu\nabla \cdot \Delta\boldsymbol{U} + \nabla \cdot \mathcal{F} = 0. \tag{5}$$

with the additional initial condition that

$$\xi_t(x,0) = \xi_1(x) \equiv -\nabla \cdot \boldsymbol{U}^0. \tag{6}$$

The GWCE shallow water model then consists of (2) and (3)-(6).

The rest of this paper is outlined as follows. In section (2) we introduce definitions and notation. In section (3), we derive a weak formulation of the GWCE-CME system of equations and state some assumptions on the solution. In section (4), we introduce the continuous-time finite element approximation to the weak solution, and derive stability and *a priori* error estimates for this approximation. In section (5), we extend these estimates to a nonlinear shallow water model. Finally, in section (6), we discuss a discrete time approximation to the linear model given above.

2. Preliminaries.

2.1. Notation. For the purposes of our analysis, we define some notation used throughout the rest of this paper.

Let Ω be a bounded polygonal domain in $\mathbb{R}^2$ and $x = (x_1, x_2) \in \mathbb{R}^2$. Moreover, let $\bar{\Omega} = \Omega \cup \partial\Omega$, where $\partial\Omega$ is the boundary of Ω.

The $\mathcal{L}^2$ inner product is denoted by

$$(\varphi, \omega) = \int_\Omega \varphi \circ \omega \, dx, \qquad \varphi, \omega \in [\mathcal{L}^2(\Omega)]^n,$$

where "$\circ$" here refers to either multiplication, dot product, or double dot product as appropriate. We will let $\langle \varphi, \omega \rangle$ denote an inner product on $\partial\Omega$. We denote the $\mathcal{L}^2$

norm by $\|\varphi\| = (\varphi,\varphi)^{1/2}$. In $\mathbb{R}^n, \alpha = (\alpha_1,\ldots,\alpha_n)$ is an n-tuple with nonnegative integer components,

$$D^\alpha = D_1^{\alpha_1}\cdots D_n^{\alpha_n} = \frac{\partial^{\alpha_1}}{\partial {x_1}^{\alpha_1}}\cdots\frac{\partial^{\alpha_n}}{\partial {x_n}^{\alpha_n}}$$

and $|\alpha| = \sum_{i=1}^n \alpha_i$.

For ℓ any nonnegative integer, let

$$\mathcal{H}^\ell \equiv \{\varphi \in \mathcal{L}^2(\Omega) \mid D^\alpha\varphi \in \mathcal{L}^2(\Omega) \text{ for } |\alpha| \le \ell\}$$

be the Sobolev space with norm

$$\|\varphi\|_{\mathcal{H}^\ell(\Omega)} = \left(\sum_{|\alpha|\le\ell} \|D^\alpha\varphi\|^2_{\mathcal{L}^2(\Omega)}\right)^{1/2}.$$

Additionally, $\mathcal{H}_0^1(\Omega)$ denotes the subspace of $\mathcal{H}^1(\Omega)$ obtained by completing $\mathcal{C}_0^\infty(\Omega)$ with respect to the norm $\|\cdot\|_{\mathcal{H}^1(\Omega)}$, where $\mathcal{C}_0^\infty(\Omega)$ is the set of infinitely differentiable functions with compact support in Ω.

Moreover, let

$$\mathcal{W}_\infty^\ell \equiv \{\varphi \in \mathcal{L}^\infty(\Omega) \mid D^\alpha\varphi \in \mathcal{L}^\infty(\Omega) \text{ for } |\alpha| \le \ell\}$$

be the Sobolev space with norm

$$\|\varphi\|_{\mathcal{W}_\infty^\ell(\Omega)} = \max_{|\alpha|\le\ell} \|D^\alpha\varphi\|_{\mathcal{L}^\infty(\Omega)}.$$

For relevant properties of these spaces, please refer to [1].

Observe, for instance, that $\mathcal{H}^\ell$ are spaces of $\mathbb{R}$-valued functions. Spaces of $\mathbb{R}^n$-valued functions will be denoted in boldface type, but their norms will not be distinguished. Thus, $\boldsymbol{\mathcal{L}^2}(\Omega) = [\mathcal{L}^2(\Omega)]^n$ has norm $\|\boldsymbol{\varphi}\|^2 = \sum_{i=1}^n \|\varphi_i\|^2$; $\boldsymbol{\mathcal{H}^1}(\Omega) = [\mathcal{H}^1(\Omega)]^n$ has norm $\|\boldsymbol{\varphi}\|^2_{\boldsymbol{\mathcal{H}^1}(\Omega)} = \sum_{i=1}^n \sum_{|\alpha|\le 1} \|D^\alpha\varphi_i\|^2$; etc. For X, a normed space with norm $\|\cdot\|_X$ and a map $f\colon [0,T] \to X$, define

$$\|f\|^2_{\mathcal{L}^2(0,T;X)} = \int_0^T \|f(\cdot,t)\|^2_X \Delta t,$$
$$\|f\|_{\mathcal{L}^\infty(0,T;X)} = \sup_{0\le t\le T} \|f(\cdot,t)\|_X.$$

2.2. Approximation Result and Inverse Estimate. Let $\mathcal{T}$ be a quasi-uniform triangulation of the polygonal domain Ω into elements E_i, $i = 1,\ldots,m$, with $\operatorname{diam}(E_i) = h_i$ and $h = \max_i h_i$. Let S_h ($\boldsymbol{S}_h$) denote a finite dimensional subspace of $\mathcal{H}^1(\Omega)$ ($\boldsymbol{\mathcal{H}}^1(\Omega)$) defined on this triangulation consisting of piecewise polynomials of degree less than s_1. Let $\boldsymbol{S}_h^g = \boldsymbol{S}_h \cap \{\boldsymbol{w} : \boldsymbol{w} = g \text{ on } \partial\Omega\}$ and $\boldsymbol{S}_h^0 = \boldsymbol{S}_h \cap \{\boldsymbol{w} : \boldsymbol{w} = 0 \text{ on } \partial\Omega\}$. Assume S_h ($\boldsymbol{S}_h$) satisfies the standard approximation property

$$\inf_{\varphi\in S_h(\boldsymbol{S}_h)} \|v-\varphi\|_{\mathcal{H}^{s_0}(\Omega)} \le K_0 h^{\ell-s_0} \|v\|_{\mathcal{H}^\ell(\Omega)}, \quad v \in \mathcal{H}^1(\Omega)\cap\mathcal{H}^\ell(\Omega), \tag{7}$$

and the inverse assumptions (see [2], Theorem 4.5.11)

$$\|\varphi\|_{\mathcal{L}^\infty(\Omega)} \le K_0 \|\varphi\|_{\mathcal{L}^2(\Omega)} h^{-1}, \quad \varphi \in S_h(\Omega), \tag{8}$$

$$\|\varphi\|_{\mathcal{H}^1(\Omega)} \le K_0 \|\varphi\|_{\mathcal{L}^2(\Omega)} h^{-1}, \quad \varphi \in S_h(\Omega). \tag{9}$$

Here, s_0 and ℓ are integers, $0 \le s_0 \le \ell < s_1$. Moreover, K_0 is a constant independent of h and v. We also define the space $\boldsymbol{S}_h^{\partial\Omega} = \boldsymbol{S}_h/\boldsymbol{S}_h^0$.

3. Weak formulation. A weak formulation of (5) is obtained as follows. From (1), we have

$$(\xi_t, v) - (\boldsymbol{U}, \nabla v) + \langle \boldsymbol{g} \cdot \nu, v \rangle = 0. \tag{10}$$

Differentiating this equation in time, holding v fixed in time, and using (2) we find

$$(\xi_{tt}, v) + (G\nabla\xi, \nabla v) - \mu(\Delta \boldsymbol{U}, \nabla v) - (\boldsymbol{\mathcal{F}}, \nabla v) + \langle \boldsymbol{g}_t \cdot \nu, v \rangle = 0, \quad v \in \mathcal{H}^1(\Omega). \tag{11}$$

Moreover, multiplying (2) by a test function and integrating by parts,

$$(\boldsymbol{U}_t, \boldsymbol{w}) + (G\nabla\xi, \boldsymbol{w}) + \mu(\nabla \boldsymbol{U}, \nabla \boldsymbol{w}) = (\boldsymbol{\mathcal{F}}, \boldsymbol{w}) + \mu\langle \nabla \boldsymbol{U} \cdot \nu, \boldsymbol{w} \rangle, \quad \boldsymbol{w} \in \boldsymbol{\mathcal{H}}^1(\Omega). \tag{12}$$

In our previous work, we were able to replace the term involving $\Delta \boldsymbol{U}$ in (11) by

$$\mu(\nabla \xi_t, \nabla v),$$

because we had assumed Dirichlet boundary conditions on ξ. From (1),

$$\Delta \xi_t = -\Delta(\nabla \cdot \boldsymbol{U}) = -\nabla \cdot \Delta \boldsymbol{U}.$$

Thus, multiplying by a test function and integrating by parts one found that

$$-(\nabla \xi_t, \nabla v) = (\Delta \boldsymbol{U}, \nabla \boldsymbol{v}),$$

if the test function was zero on $\partial\Omega$. Here, because our test function v is not zero on the boundary, we cannot make this substitution in (11) without introducing a boundary term involving ξ. This term $\nabla \xi_t \cdot \nu$ is unknown.

In defining our method below, we handle the $\Delta \boldsymbol{U}$ term in (11) without requiring additional continuity on the finite element space. We will approximate quantities, ξ, $\boldsymbol{U}$, $\Delta \boldsymbol{U}$ on Ω and $\boldsymbol{\lambda} \equiv \nabla \boldsymbol{U} \cdot \nu$ on $\partial\Omega$. The equations for ξ and $\boldsymbol{U}$ are derived from (11) and (12). Integration by parts yields an equation for $\Delta \boldsymbol{U}$

$$(\Delta \boldsymbol{U}, \boldsymbol{w}) = -(\nabla \boldsymbol{U}, \nabla \boldsymbol{w}) + \langle \boldsymbol{\lambda}, \boldsymbol{w} \rangle, \quad \boldsymbol{w} \in \boldsymbol{\mathcal{H}}^1(\Omega). \tag{13}$$

And finally, by (12), we have an equation for $\boldsymbol{\lambda}$

$$\mu\langle \boldsymbol{\lambda}, \boldsymbol{w} \rangle = (\boldsymbol{U}_t, \boldsymbol{w}) + (G\nabla\xi, \boldsymbol{w}) + \mu(\nabla \boldsymbol{U}, \nabla \boldsymbol{w}) - (\boldsymbol{\mathcal{F}}, \boldsymbol{w}), \quad \boldsymbol{w} \in \boldsymbol{\mathcal{H}}^1(\Omega). \tag{14}$$

3.1. Some Assumptions. We will make the following assumptions about the solutions and the data. First, we assume the domain Ω is polygonal, and for $(\boldsymbol{x}, t) \in \bar{\Omega} \times (0, T]$,

A1. the solutions $\xi, \boldsymbol{U}$ to (2) and (3)-(6) exist and are unique,

A2. μ is a positive constant,

We make the following smoothness assumptions on the initial data and on the solutions.

A3. $\xi^0, \boldsymbol{U}^0(\boldsymbol{x}) \in \mathcal{H}^{\ell}(\Omega)$,

A4. $\xi \in \mathcal{H}^{\ell+1}(\Omega), \ t > 0$,

A5. $\boldsymbol{U}, \boldsymbol{U}_t \in \boldsymbol{\mathcal{H}}^{\ell}(\Omega), \ t > 0$,

A6. $\Delta \boldsymbol{U} \in \boldsymbol{\mathcal{H}}^{\ell}(\Omega), \ t > 0$,

A7. $\boldsymbol{\lambda} \in \boldsymbol{\mathcal{L}}^2(\partial\Omega), \ t > 0$,

where the integer $\ell \geq 2$ is defined in the next section.

4. A Galerkin Finite Element Approximation.

4.1. The Continuous-Time Galerkin Approximation. Define an approximation $\xi_h(\cdot,t) \in \mathcal{S}_h$ by

$$(\xi_h(\cdot,0),v) = (\xi^0,v), \quad v \in \mathcal{S}_h, \tag{15}$$

$$((\xi_h)_t(\cdot,0),v) = (\xi_h^1,v) = -(\nabla\cdot \boldsymbol{U}_h(\cdot,0),v), \quad v \in \mathcal{S}_h, \tag{16}$$

and for $t > 0$,

$$\begin{aligned}&((\xi_h)_{tt},v) + (G\pi(\nabla\xi_h),\nabla v)\\ &\quad - \mu(\Delta_h \boldsymbol{U}_h,\nabla v) - (\boldsymbol{\mathcal{F}},\nabla v) + \langle \boldsymbol{g}_t\cdot\nu, v\rangle = 0, \quad v \in \mathcal{S}_h,\end{aligned} \tag{17}$$

where $\pi(\nabla\xi_h)$ denotes the L^2 projection of $\nabla\xi_h$ into $\boldsymbol{\mathcal{S}}_h$, and $\Delta_h \boldsymbol{U}_h$ is defined below.

Define an approximation $\boldsymbol{U}_h(\cdot,t) \in \boldsymbol{\mathcal{S}}_h^g$ by

$$(\nabla \boldsymbol{U}_h(\cdot,0),\nabla \boldsymbol{w}) = (\nabla \boldsymbol{U}^0,\nabla \boldsymbol{w}), \quad \boldsymbol{w} \in \boldsymbol{\mathcal{S}}_h^0, \tag{18}$$

and for $t > 0$,

$$((\boldsymbol{U}_h)_t,\boldsymbol{w}) + (G\nabla\xi_h,\boldsymbol{w}) + \mu(\nabla \boldsymbol{U}_h,\nabla \boldsymbol{w}) = (\boldsymbol{\mathcal{F}},\boldsymbol{w}), \quad \boldsymbol{w} \in \boldsymbol{\mathcal{S}}_h^0. \tag{19}$$

The "discrete Laplacian" $\Delta_h \boldsymbol{U}_h \in \boldsymbol{\mathcal{S}}_h$ in (17) is defined by

$$(\Delta_h \boldsymbol{U}_h,\boldsymbol{w}) = -(\nabla \boldsymbol{U}_h,\nabla \boldsymbol{w}) + \langle \boldsymbol{\lambda}_h,\boldsymbol{w}\rangle, \quad \boldsymbol{w} \in \boldsymbol{\mathcal{S}}_h, \tag{20}$$

where the approximate boundary flux $\boldsymbol{\lambda}_h \in \boldsymbol{\mathcal{S}}_h^{\partial\Omega}$ is defined by

$$\begin{aligned}\mu\langle \boldsymbol{\lambda}_h,\boldsymbol{w}_b\rangle &= ((\boldsymbol{U}_h)_t,\boldsymbol{w}_b) + (G\nabla\xi_h,\boldsymbol{w}_b)\\ &\quad +\mu(\nabla \boldsymbol{U}_h,\nabla \boldsymbol{w}_b) - (\boldsymbol{\mathcal{F}},\boldsymbol{w}_b), \quad \boldsymbol{w}_b \in \boldsymbol{\mathcal{S}}_h^{\partial\Omega}.\end{aligned} \tag{21}$$

Thus, the system (15)–(21) yields a system of equations in four unknowns, ξ_h, $\boldsymbol{U}_h$, $\Delta_h \boldsymbol{U}_h$ and $\boldsymbol{\lambda}_h$.

In section (6), we will formulate a discrete time version of this scheme and show that these unknowns can be determined in a sequential manner. Moreover, all matrices which arise are symmetric, positive definite, and time-independent.

4.2. A stability estimate. As a prelude to deriving an error estimate, we study the stability of the scheme above in the case $\boldsymbol{g} = 0$ and $\boldsymbol{\mathcal{F}} = 0$.

We first manipulate the equations above to yield an equation for elevation. Integrating (17), (19), (20) and (21) in time from zero to t, we obtain

$$((\xi_h)_t,v) + (\int_0^t G\pi(\nabla\xi_h)ds,\nabla v) - \mu(\int_0^t \Delta_h \boldsymbol{U}_h ds,\nabla v) = (\xi_h^1,v), \quad v \in \mathcal{S}_h, \tag{22}$$

$$(\boldsymbol{U}_h,\boldsymbol{w}) + (\int_0^t G\nabla\xi_h ds,\boldsymbol{w}) + \mu(\int_0^t \nabla \boldsymbol{U}_h ds,\nabla \boldsymbol{w}) = (\boldsymbol{U}^0,\boldsymbol{w}), \quad \boldsymbol{w} \in \boldsymbol{\mathcal{S}}_h^0, \tag{23}$$

$$(\int_0^t \Delta_h \boldsymbol{U}_h ds,\boldsymbol{w}) = -(\int_0^t \nabla \boldsymbol{U}_h ds,\nabla \boldsymbol{w}) + \langle \int_0^t \boldsymbol{\lambda}_h ds,\nabla \boldsymbol{w}\rangle, \quad \boldsymbol{w} \in \boldsymbol{\mathcal{S}}_h, \tag{24}$$

$$(25)\qquad \mu\langle\int_0^t \boldsymbol{\lambda}_h ds, \boldsymbol{w}_b\rangle = (\boldsymbol{U}_h, \boldsymbol{w}_b) + (\int_0^t G\nabla\xi_h ds, \boldsymbol{w}_b) + \mu(\int_0^t \nabla \boldsymbol{U}_h ds, \nabla \boldsymbol{w}_b) - (\boldsymbol{U}^0, \boldsymbol{w}_b), \quad \boldsymbol{w}_b \in \boldsymbol{S}_h^{\partial\Omega}.$$

Adding (23) and (25) we find

$$(26)\qquad (\boldsymbol{U}_h, \boldsymbol{w}+\boldsymbol{w}_b) + (\int_0^t G\nabla\xi_h ds, \boldsymbol{w}+\boldsymbol{w}_b) + \mu(\int_0^t \nabla \boldsymbol{U}_h ds, \nabla(\boldsymbol{w}+\boldsymbol{w}_b)) - \mu\langle\int_0^t \boldsymbol{\lambda}_h ds, \boldsymbol{w}+\boldsymbol{w}_b\rangle = (\boldsymbol{U}^0, \boldsymbol{w}+\boldsymbol{w}_b).$$

Here we have used the fact that $\boldsymbol{w} = 0$ on $\partial\Omega$ in the term involving $\boldsymbol{\lambda}_h$.

We now set $\boldsymbol{w} + \boldsymbol{w}_b = \pi(\nabla\xi_h)$ in (26), and set $v = \xi_h$ in (22) to obtain

$$(27)\qquad ((\xi_h)_t, \xi_h) + (\int_0^t G\pi(\nabla\xi_h)ds, \nabla\xi_h) - \mu(\int_0^t \Delta_h \boldsymbol{U}_h ds, \nabla\xi_h) = (\xi_h^1, \xi_h),$$

and

$$(28)\qquad (\boldsymbol{U}_h, \nabla\xi_h) + (\int_0^t G\nabla\xi_h ds, \pi(\nabla\xi_h)) + \mu(\int_0^t \nabla \boldsymbol{U}_h, \nabla\pi(\nabla\xi_h)) - \mu\langle\int_0^t \boldsymbol{\lambda}_h ds, \pi(\nabla\xi_h)\rangle = (\boldsymbol{U}_h(\cdot,0), \nabla\xi_h).$$

Setting $\boldsymbol{w} = \pi(\nabla\xi_h)$ in (24), we find

$$(\int_0^t \Delta_h \boldsymbol{U}_h ds; \nabla\xi_h) = (\int_0^t \Delta_h \boldsymbol{U}_h ds, \pi(\nabla\xi_h)) = -(\int_0^t \nabla \boldsymbol{U}_h ds, \nabla\pi(\nabla\xi_h)) + \langle\int_0^t \boldsymbol{\lambda}_h ds, \pi(\nabla\xi_h)\rangle.$$

Substituting this result into (28) and subtracting from (27), we obtain a useful equation for elevation.

$$(29)\qquad ((\xi_h)_t, \xi_h) = (\boldsymbol{U}_h, \nabla\xi_h) - (\int_0^t G\pi(\nabla\xi_h)ds, \nabla\xi_h) + (\int_0^t G\nabla\xi_h ds, \pi(\nabla\xi_h)) + (\xi_h^1, \xi_h) - (\boldsymbol{U}_h(\cdot,0), \nabla\xi_h) = (\boldsymbol{U}_h, \nabla\xi_h) + (\xi_h^1, \xi_h) - (\boldsymbol{U}_h(\cdot,0), \nabla\xi_h).$$

We continue by deriving an equation for velocity. Letting $\boldsymbol{w} = \boldsymbol{U}_h$ in (19) we obtain

$$(30)\qquad ((\boldsymbol{U}_h)_t, \boldsymbol{U}_h) + \mu(\nabla \boldsymbol{U}_h, \nabla \boldsymbol{U}_h) = -(G\nabla\xi_h, \boldsymbol{U}_h).$$

Now, adding (29) and (30) and integrating by parts we find

$$(31)\qquad ((\xi_h)_t, \xi_h) + ((\boldsymbol{U}_h)_t, \boldsymbol{U}_h) + \mu(\nabla \boldsymbol{U}_h, \nabla \boldsymbol{U}_h) = (\xi_h^1, \xi_h) - (\nabla\cdot \boldsymbol{U}_h, \xi_h) + (G\xi_h, \nabla\cdot \boldsymbol{U}_h) + (\nabla\cdot \boldsymbol{U}_h(\cdot,0), \xi_h) = -(\nabla\cdot \boldsymbol{U}_h, \xi_h) + (G\xi_h, \nabla\cdot \boldsymbol{U}_h),$$

where in the last step we have used the fact that ξ_h^1 is the L^2 projection of $-\nabla\cdot\boldsymbol{U}_h(\cdot,0)$ into $\mathcal{S}_h$.

Integrating (31) in time from 0 to T we find

$$||\xi_h(\cdot,T)||^2+||\boldsymbol{U}_h(\cdot,T)||^2+2\mu\int_0^T||\nabla\boldsymbol{U}_h||^2dt$$
$$\leq||\xi^0||^2+||\boldsymbol{U}^0||^2+\int_0^T\left[\mu||\nabla\boldsymbol{U}_h||^2+C||\xi_h||^2\right]dt.$$

An application of Gronwall's Lemma gives the following result.

LEMMA 4.1. *For the case $g=0$ and $\mathcal{F}=0$, and any $T>0$,*

$$||\xi_h(\cdot,T)||+||\boldsymbol{U}_h(\cdot,T)||\leq C\left(||\xi^0||+||\boldsymbol{U}^0||\right). \tag{32}$$

4.3. An *a priori* error estimate. We now consider the more general case where g and $\mathcal{F}$ are not zero. In order to derive an error estimate, let $\tilde{\xi}_h$ denote the L^2 projection of ξ into $\mathcal{S}_h$, and $\tilde{\mathbf{U}}_h$ the elliptic projection of $\boldsymbol{U}$ into $\boldsymbol{\mathcal{S}}_h^g$; that is, $\tilde{\mathbf{U}}_h\in\boldsymbol{\mathcal{S}}_h^g$ is defined by

$$(\nabla(\tilde{\mathbf{U}}_h-\boldsymbol{U}),\nabla\boldsymbol{w})=0,\quad \boldsymbol{w}\in\boldsymbol{\mathcal{S}}_h^0. \tag{33}$$

Let $\psi_\xi=\xi_h-\tilde{\xi}_h$, $\boldsymbol{\psi}_U=\boldsymbol{U}_h-\tilde{\mathbf{U}}_h$, $\theta_\xi=\xi-\tilde{\xi}_h$, and $\boldsymbol{\theta}_U=\boldsymbol{U}-\tilde{\mathbf{U}}_h$.

We first derive an equation for ψ_ξ. Integrating (11) in time and combining with (22) we find

$$((\psi_\xi)_t,v)+(\int_0^t G\pi(\nabla\xi_h)ds,\nabla v)$$
$$=(\xi_h^1-\xi_t(\cdot,0),v)+((\theta_\xi)_t,v)+(\int_0^t G\nabla\xi ds,\nabla v)$$
$$+\mu(\int_0^t(\Delta_h\boldsymbol{U}_h-\Delta\boldsymbol{U})ds,\nabla v). \tag{34}$$

Integrating (12) and (14) in time, adding them and combining with (26), we find

$$(\boldsymbol{\psi}_U,\boldsymbol{w}+\boldsymbol{w}_b)+(\int_0^t G\nabla\xi_h ds,\boldsymbol{w}+\boldsymbol{w}_b)$$
$$=(\boldsymbol{\theta}_U,\boldsymbol{w}+\boldsymbol{w}_b)-(\boldsymbol{\theta}_U(\cdot,0),\boldsymbol{w}+\boldsymbol{w}_b)+(\int_0^t G\nabla\xi ds,\boldsymbol{w}+\boldsymbol{w}_b)$$
$$+\mu(\int_0^t(\Delta_h\boldsymbol{U}_h-\Delta\boldsymbol{U})ds,\boldsymbol{w}+\boldsymbol{w}_b). \tag{35}$$

Here we have used (20) and (13) in the last term.

Setting $v=\psi_\xi$ in (34) and $\boldsymbol{w}+\boldsymbol{w}_b=\pi(\nabla\psi_\xi)$ in (35), where $\pi(\nabla\psi_\xi)$ is the L^2 projection of $\nabla\psi_\xi$ into $\boldsymbol{\mathcal{S}}_h$, and subtracting (35) from (34), we find a desired equation for ψ_ξ.

$$((\psi_\xi)_t,\psi_\xi)=(\boldsymbol{\psi}_U,\nabla\psi_\xi)-(\int_0^t G\nabla\xi ds,\pi(\nabla\psi_\xi)-\nabla\psi_\xi)$$
$$+((\theta_\xi)_t,\psi_\xi)-(\boldsymbol{\theta}_U,\pi(\nabla\psi_\xi))+(\boldsymbol{\theta}_U(\cdot,0),\pi(\nabla\psi_\xi))$$
$$+\mu(\int_0^t\Delta\boldsymbol{U}ds,\pi(\nabla\psi_\xi)-\nabla\psi_\xi))-(\nabla\cdot(\boldsymbol{U}_h-\boldsymbol{U})(\cdot,0),\psi_\xi). \tag{36}$$

We continue by deriving an equation for ψ_U. From (19), we find

$$(37)\qquad \begin{aligned}&((\psi_U)_t, \psi_U) + (G\nabla\psi_\xi, \psi_U) + \mu(\nabla\psi_U, \nabla\psi_U)\\ &= ((\theta_U)_t, \psi_U) + (G\nabla\theta_\xi, \psi_U) + \mu(\nabla\theta_U, \nabla\psi_U).\end{aligned}$$

Adding (36)-(37), integrating by parts, and using the definitions of the L^2 and elliptic projections, we find

$$\begin{aligned}(38)\qquad &((\psi_\xi)_t, \psi_\xi) + ((\psi_U)_t, \psi_U) + \mu(\nabla\psi_U, \nabla\psi_U)\\ &= -(\nabla\cdot\psi_U, \psi_\xi) - (\int_0^t G(\nabla\xi - \pi(\nabla\xi))ds, \pi(\nabla\psi_\xi) - \nabla\psi_\xi)\\ &\quad - (\theta_U, \pi(\nabla\psi_\xi)) + (\theta_U(\cdot,0), \pi(\nabla\psi_\xi)) + ((\theta_U)_t, \psi_U)\\ &\quad + (G(\psi_\xi - \theta_\xi), \nabla\cdot\psi_U) + \mu(\int_0^t (\Delta U - \pi(\Delta U))ds, \pi(\nabla\psi_\xi) - \nabla\psi_\xi)\\ &\quad - (\nabla\cdot(U_h - U)(\cdot,0), \psi_\xi),\end{aligned}$$

where $\pi(\Delta U)$ is the L^2 projection of ΔU into S_h.

Integrating this equation in time, and bounding terms on the right hand side, we find

$$\begin{aligned}(39)\qquad &||\psi_\xi(\cdot,T)||^2 + ||\psi_U(\cdot,T)||^2 + 2\mu\int_0^T ||\nabla\psi_U||^2 dt\\ &\le \mu\int_0^T ||\nabla\psi_U||^2 dt + Ch^{-2}\int_0^T ||\nabla\xi - \pi(\nabla\xi)||^2 dt\\ &\quad + C\int_0^T \left[||\theta_\xi||^2 + ||\psi_\xi||^2\right] dt\\ &\quad + C\int_0^T \left[h^{-2}||\theta_U||^2 + ||(\theta_U)_t||^2 + ||\psi_U||^2\right] dt + Ch^{-2}||\theta_U(\cdot,0)||^2\\ &\quad + Ch^{-2}\int_0^T ||\Delta U - \pi(\Delta U)||^2 dt + Ch^2\int_0^T \left[||\pi(\nabla\psi_\xi)||^2 + ||\nabla\psi_\xi||^2\right] dt\\ &\quad + C||\nabla\cdot(U_h(\cdot,0) - U(\cdot,0))||^2.\end{aligned}$$

It is easily shown that

$$||\pi(\nabla\psi_\xi)|| \le ||\nabla\psi_\xi||.$$

This result together with inverse estimate (9) yields

$$Ch^2\int_0^T \left[||\pi(\nabla\psi_\xi)||^2 + ||\nabla\psi_\xi||^2\right] dt \le C\int_0^T ||\psi_\xi||^2 dt.$$

Combining the above with (39) as well as the approximation result (7) yields

$$\begin{aligned}&||\psi_\xi(\cdot,T)||^2 + ||\psi_U(\cdot,T)||^2 + \mu\int_0^T ||\nabla\psi_U||^2 dt\\ &\le Ch^{2(l-1)} + C\int_0^T \left[||\psi_\xi||^2 + ||\psi_U||^2\right] dt.\end{aligned}$$

Applying Gronwall's inequality and the triangle inequality, we obtain the following result.

THEOREM 4.2. *Let the assumptions* **A1-A7** *hold. Assume the finite element solutions* ξ_h, U_h, $\Delta_h U_h$, *and* λ_h *to (15)-(21) exist and are unique. Then there exists a constant* C *independent of* h *such that*

$$\|(U - U_h)\|_{\mathcal{L}^\infty(0,T;\mathcal{L}^2)} + \|\xi - \xi_h\|_{\mathcal{L}^\infty(0,T;\mathcal{L}^2)} \leq Ch^{l-1}. \tag{40}$$

We remark that this rate of convergence is the same as that obtained in our earlier paper [3].

5. A nonlinear model. Realistic shallow water models are nonlinear. For example, the term $G\nabla\xi$ in the momentum equation (2) is actually $gH\nabla\xi$, where g is gravitational acceleration (assumed constant). Moreover, an advection term $\nabla\cdot U^2/H$ is also present. There are also forcing terms (Coriolis force, wind stress, tide potentials, bottom friction) present in the equation; we will assume these are known, and for simplicity lump them into the term $\mathcal{F}$. Thus (2) becomes

$$U_t + gH\nabla\xi + \nabla\cdot\frac{U^2}{H} - \mu\Delta U = \mathcal{F}, \tag{41}$$

and the GWCE (5) becomes

$$\xi_{tt} - \nabla\cdot(gH\nabla\xi) - \nabla\cdot\left(\nabla\cdot\frac{U^2}{H}\right) + \mu\nabla\cdot\Delta U + \nabla\cdot\mathcal{F} = 0. \tag{42}$$

Let

$$\Gamma = gH\nabla\xi + \nabla\cdot\frac{U^2}{H},$$

and

$$\Gamma_h = gH_h\nabla\xi_h + \nabla\cdot\frac{U_h^2}{H_h},$$

where

$$H_h = h_b + \xi_h.$$

Let $\pi\Gamma_h$ ($\pi\Gamma$) denote the L^2 projection of Γ_h (Γ) into S_h. Our finite element method is defined as follows. We choose the initial data as before and define the discrete Laplacian by (20). Then, for $t > 0$,

$$\begin{aligned}&((\xi_h)_{tt}, v) + (\pi\Gamma_h, \nabla v)\\ &\quad - \mu(\Delta_h U_h, \nabla v) - (\mathcal{F}, \nabla v) + \langle g_t\cdot\nu, v\rangle = 0, \quad v \in S_h,\end{aligned} \tag{43}$$

$$\begin{aligned}((U_h)_t, w) + \mu(\nabla U_h, \nabla w) &= -(\Gamma_h, w) + (\mathcal{F}, w)\\ &= -(\pi\Gamma_h, w) + (\mathcal{F}, w), \quad w \in S_h^0,\end{aligned} \tag{44}$$

and

$$\begin{aligned}\mu(\lambda_h, w_b) &= ((U_h)_t, w_b) + (\Gamma_h, w_b)\\ &\quad +\mu(\nabla U_h, \nabla w_b) - (\mathcal{F}, w_b), \quad w_b \in S_h^{\partial\Omega}.\end{aligned} \tag{45}$$

For the error analysis below, we will assume that a constant K exists such that

A8. $||\xi_h||_{\mathcal{L}^\infty(0,T;\mathcal{L}^\infty)} + ||U_h||_{\mathcal{L}^\infty(0,T;\mathcal{L}^\infty)} \leq K$,
and that positive constants H_{**}, H^{**} exist such that

A8. $H_{**} < H_h < H^{**}$.

Using an induction argument as in [3], one can show that K, H_{**} and H^{**} are independent of h for h sufficiently small, for polynomials of degree two and higher. We will also assume that

A9. $\xi, h_b, U \in \mathcal{W}^1_\infty(\Omega), \Gamma \in \mathcal{H}^t(\Omega)$.

Define ψ_ξ, ψ_U, θ_ξ and θ_U as before. We first derive an equation for ψ_ξ. Integrate (43) in time and subtract the analogous equation obtained from (42) to find

$$
\begin{aligned}
(46) \qquad ((\psi_\xi)_t, v) &= (\xi_h^1 - \xi_t(\cdot,0), v) + (\int_0^t \pi(\Gamma - \Gamma_h)ds, \nabla v) \\
&\quad + ((\theta_\xi)_t, v) + (\int_0^t (\Gamma - \pi\Gamma)ds, \nabla v) \\
&\quad + \mu(\int_0^t (\Delta_h U_h - \Delta U)ds, \nabla v), \quad v \in S_h.
\end{aligned}
$$

Integrate (44) and (45) in time and subtract the analogous equation obtained from (41) to find

$$
\begin{aligned}
(47) \quad (\psi_U, \boldsymbol{w}) &= (\int_0^t \pi(\Gamma - \Gamma_h)ds, \boldsymbol{w}) + \mu(\int_0^t (\Delta_h U_h - \Delta U)ds, \boldsymbol{w}) + (\theta_U, \boldsymbol{w}) \\
&\quad - (\theta_U(\cdot,0), \boldsymbol{w}), \quad \boldsymbol{w} \in \boldsymbol{S}_h.
\end{aligned}
$$

Setting $v = \psi_\xi$ in (46), $\boldsymbol{w} = \pi(\nabla\psi_\xi)$ in (47), subtracting (47) from (46), and using the definition of the L^2 projections, yields

$$
\begin{aligned}
(48) \ ((\psi_\xi)_t, \psi_\xi) &= (\psi_U, \nabla\psi_\xi) + (\int_0^t (\Gamma - \pi\Gamma)ds, \nabla\psi_\xi) \\
&\quad + (\xi_h^1 - \xi_t(\cdot,0), \psi_\xi) + \mu(\int_0^t (\Delta U - \pi(\Delta U))ds, \pi(\nabla\psi_\xi) - \nabla\psi_\xi) \\
&\quad - (\theta_U, \pi\nabla\psi_\xi) + (\theta_U(\cdot,0), \pi\nabla\psi_\xi)
\end{aligned}
$$

We continue by deriving an equation for ψ_U. From (44) and (41), and the definition of the elliptic projection, we obtain

$$
(49) \qquad ((\psi_U)_t, \boldsymbol{w}) + \mu(\nabla\psi_U, \nabla\boldsymbol{w}) = (\Gamma - \Gamma_h, \boldsymbol{w}) + ((\theta_U)_t, \boldsymbol{w}), \quad \boldsymbol{w} \in \boldsymbol{S}_h^0.
$$

Now, adding (48) and (49), we obtain

$$
\begin{aligned}
(50) \quad &((\psi_\xi)_t, \psi_\xi) + ((\psi_U)_t, \psi_U) + \mu(\nabla\psi_U, \nabla\psi_U) \\
&= (\xi_h^1 - \xi_t(\cdot,0), \psi_\xi) + (\psi_U, \nabla\psi_\xi) + \mu(\int_0^t (\Delta U - \pi(\Delta U))ds, \pi(\nabla\psi_\xi) - \nabla\psi_\xi) \\
&\quad + (\int_0^t (\Gamma - \pi\Gamma)ds, \nabla\psi_\xi) - (\theta_U, \pi\nabla\psi_\xi) + (\theta_U(\cdot,0), \pi\nabla\psi_\xi) \\
&\quad + (\Gamma - \Gamma_h), \psi_U) + ((\theta_U)_t, \psi_U).
\end{aligned}
$$

The fourth and seventh terms on the right side of (50) are handled as follows.

$$(51)\qquad (\int_0^t (\Gamma - \pi\Gamma)ds, \nabla\psi_\xi) \le Ch^{-2}||\int_0^t (\Gamma - \pi\Gamma)ds||^2 + Ch^2||\nabla\psi_\xi||^2$$
$$\le Ch^{2(l-1)} + C||\psi_\xi||^2.$$

$$(52)\qquad (\Gamma - \Gamma_h, \psi_U) = (gH\nabla\xi - gH_h\nabla\xi_h, \psi_U) + (\nabla\cdot(\frac{U^2}{H} - \frac{U_h^2}{H_h}), \psi_U)$$
$$= (gh_b\nabla(\xi - \xi_h), \psi_U) + \frac{g}{2}(\nabla\xi^2 - \nabla\xi_h^2, \psi_U)$$
$$-(\frac{U^2}{H} - \frac{U_h^2}{H_h}, \nabla\psi_U)$$
$$= -g(\xi - \xi_h, \nabla\cdot(h_b\psi_U)) - \frac{g}{2}(\xi^2 - \xi_h^2, \nabla\cdot\psi_U)$$
$$-(\frac{U^2H_h - U_h^2H}{HH_h}, \nabla\psi_U)$$
$$= -g(\xi - \xi_h, \nabla\cdot(h_b\psi_U)) - \frac{g}{2}(\xi^2 - \xi_h^2, \nabla\cdot\psi_U)$$
$$-(\frac{U^2(H_h - H) - H_h(U^2 - U_h^2)}{HH_h}, \nabla\psi_U)$$
$$\le C||\psi_\xi||^2 + C||\theta_\xi||^2 + C||\psi_U||^2$$
$$+C||\theta_U||^2 + \frac{\mu}{2}||\nabla\psi_U||^2.$$

Combining (50), (51) and (52), choosing ϵ sufficiently small, using bounds previously derived for the remaining terms, and integrating in time, we obtain

$$(53)\qquad ||\psi_\xi(\cdot,T)||^2 + ||\psi_U(\cdot,T)||^2 + \mu\int_0^T ||\nabla\psi_U||^2dt$$
$$\le Ch^{2(l-1)} + C\int_0^T \left[||\psi_\xi||^2 + ||\psi_U||^2\right]dt.$$

Using Gronwall's Lemma we obtain the following.

THEOREM 5.1. *Assume the finite element solutions ξ_h, U_h, $\Delta_h U_h$, and λ_h to (15), (16), (43), (18), (44), (20) and (45) exist and are unique. Let the assumptions* **A1-A10** *hold and assume h is sufficiently small. Then, there exists a constant C independent of h such that*

$$(54)\qquad ||U - U_h||_{\mathcal{L}^\infty(0,T;\mathcal{L}^2)} + ||\xi - \xi_h||_{\mathcal{L}^\infty(0,T;\mathcal{L}^2)} \le Ch^{l-1}.$$

6. A Discrete-Time Galerkin Approximation. In this section, we return for simplicity to the linear model presented in Section 1, with $g = \mathcal{F} = 0$, and formulate a discrete time method. We extend our continuous-time stability argument presented in section (4) and show that the discrete scheme satisfies the same stability bound. We leave the derivation of error estimates for this scheme to the reader.

Choose a time step $\Delta t > 0$ and set $t^k = k\Delta t$, $k = 0, 1, \ldots$. Denote $f(x, t^k)$ by f^k. A discrete time scheme based on (2) and (3)-(6) can be defined as follows. We define

the initial approximations ξ_h^0 and U_h^0 as before, see (15), (18). We enforce the initial condition (6) by

$$(55) \qquad (\frac{\xi_h^1 - \xi_h^0}{\Delta t}, v) + (\nabla \cdot U_h^0, v) = 0, \quad v \in S_h.$$

(Note that here, ξ_h^1 has a different meaning than in the previous sections, it is defined by (55).) Then, for $k = 1, 2, \ldots$,

$$(56) \qquad (\frac{U_h^k - U_h^{k-1}}{\Delta t}, w) + (G\nabla\xi_h^k, w) + \mu(\nabla U_h^k, \nabla w) = 0, \quad w \in S_h^0,$$

$$(57) \qquad \mu\langle\lambda_h^k, w_b\rangle = (\frac{U_h^k - U_h^{k-1}}{\Delta t}, w_b) + (G\nabla\xi_h^k, w_b) + \mu(\nabla U_h^k, \nabla w_b), \quad w_b \in S_h^{\partial\Omega},$$

$$(58) \qquad (\Delta_h U_h^k, w) = -(\nabla U_h^k, \nabla w) + \langle\lambda_h^k, w\rangle, \quad w \in S_h,$$

and

$$(59) \qquad (\frac{\xi_h^{k+1} - 2\xi_h^k + \xi_h^{k-1}}{\Delta t^2}, v) + (G\pi(\nabla\xi_h^k), \nabla v) - \mu(\Delta_h U_h^k, \nabla v) = 0, \quad v \in S_h.$$

Note that, at each step in the above procedure, the matrices which arise are symmetric and positive definite, and independent of time.

We now extend the stability argument given above for the continuous time scheme to this discrete scheme. This argument can also be used to show uniqueness (hence existence) for the solutions to the system give above.

We first derive an equation for ξ_h^{n+1}. Adding (56) and (58) and using the definition (58) of $\Delta_h U_h^k$, we find

$$(60) \qquad (\frac{U_h^k - U_h^{k-1}}{\Delta t}, w) + (G\nabla\xi_h^k, w) - \mu(\Delta_h U_h^k, w) = 0, \quad w \in S_h.$$

Multiplying this equation by Δt and summing on k, $k = 1, \ldots, n$, for some integer $n > 0$, we find

$$(61) \quad (U_h^n, w) + (\sum_{k=1}^{n} G\nabla\xi_h^k \Delta t, w) - \mu(\sum_{k=1}^{n} \Delta_h U_h^k \Delta t, w) = (U_h^0, w), \quad w \in S_h.$$

Multiplying (59) by Δt and summing on k we obtain

$$(62) \qquad (\frac{\xi_h^{n+1} - \xi_h^n}{\Delta t}, v) + (\sum_{k=1}^{n} G\pi(\nabla\xi_h^k)\Delta t, \nabla v) - \mu(\sum_{k=1}^{n} \Delta_h U_h^k \Delta t, \nabla v) = (\frac{\xi_h^1 - \xi_h^0}{\Delta t}, v), \quad v \in S_h.$$

Setting $v = \xi_h^{n+1}$ in (62) and $w = \pi(\nabla\xi_h^{n+1})$ in (61), subtracting (61) from (62) and substituting (55), we find

$$(63) \qquad (\frac{\xi_h^{n+1} - \xi_h^n}{\Delta t}, \xi_h^{n+1}) = -(U_h^0, \nabla\xi_h^{n+1}) - (\nabla \cdot U_h^0, \xi_h^{n+1}) + (U_h^n, \nabla\xi_h^{n+1}).$$

We continue by deriving an equation for U_h^n. Setting $k = n$ in (56) and $w = U_h^n$, we obtain

$$(64) \qquad (\frac{U_h^n - U_h^{n-1}}{\Delta t}, U_h^n) + \mu ||\nabla U_h^n||^2 = -(G\nabla \xi_h^n, U_h^n).$$

Now, adding (63) and (64), using the inequality $a(a-b) \geq (a^2 - b^2)/2$, and integrating by parts we find

$$(65) \qquad \frac{||\xi_h^{n+1}||^2 - ||\xi_h^n||^2}{2\Delta t} + \frac{||U_h^n||^2 - ||U_h^{n-1}||^2}{2\Delta t} + \mu ||\nabla U_h^n||^2 \leq (G\xi_h^n, \nabla \cdot U_h^n) - (\nabla \cdot U_h^n, \xi_h^{n+1}).$$

Multiplying (65) by $2\Delta t$ and summing on n, $n = 1, 2, \ldots, N$ where $N \geq 1$ is an integer, we find

$$(66) \qquad ||\xi_h^{N+1}||^2 + ||U_h^N||^2 + 2\mu \sum_{n=1}^{N} ||\nabla U_h^n||^2 dt \leq ||\xi_h^1||^2 + ||U_h^0||^2 + C \sum_{n=1}^{N+1} ||\xi_h^n||^2 \Delta t + \mu \sum_{n=1}^{N} ||\nabla U_h^n||^2 \Delta t.$$

Finally, we note that, by (55), setting $v = \xi_h^1$ we find

$$(67) \qquad ||\xi_h^1|| \leq ||\xi_h^0|| + \Delta t ||\nabla \cdot U_h^0||.$$

Combining (67) with (66) and applying the discrete version of Gronwall's inequality we obtain the following.

LEMMA 6.1. *For the case $g = 0$ and $\mathcal{F} = 0$, N a positive integer and $\Delta t > 0$,*

$$(68) \qquad ||\xi_h^N|| + ||U_h^N|| \leq C \left(||\xi_h^0|| + ||U_h^0|| + \Delta t ||\nabla \cdot U_h^0|| \right).$$

REFERENCES

[1] R. A. ADAMS, *Sobolev Spaces*, vol. 65 of Pure and Applied Mathematics, Academic Press, New York, 1978.

[2] S. C. BRENNER AND L. R. SCOTT, *The Mathematical Theory of Finite Element Methods*, vol. 15 of Texts in Applied Mathematics, Springer-Verlag, New York, 1994.

[3] S. CHIPPADA, C. N. DAWSON, M. L. MARTÍNEZ, AND M. F. WHEELER, *Finite element approximations to the system of shallow water equations, Part I: Continuous time a priori error estimates*, Tech. Report TICAM Report 95-18, University of Texas, Austin, TX 78712, December 1995. To appear in SINUM.

[4] ———, *Finite element approximations to the system of shallow water equations, Part II: Discrete time a priori error estimates*, Tech. Report TICAM Report 96-34, University of Texas, Austin, TX 78712, December 1996. To appear in SINUM.

[5] I. P. E. KINNMARK, *The Shallow Water Wave Equations: Formulation, Analysis and Applications*, vol. 15 of Lecture Notes in Engineering, Springer-Verlag, New York, 1985.

[6] R. L. KOLAR, J. J. WESTERINK, M. E. CANTEKIN, AND C. A. BLAIN, *Aspects of nonlinear simulations using shallow water models based on the wave continuity equation*, Computers and Fluids, ?? (1994), p. ??

[7] R. A. LUETTICH, J. J. WESTERINK, AND N. W. SCHEFFNER, ADCIRC: *An advanced three-dimensional circulation model for shelves, coasts, and estuaries*, Tech. Report 1, Department of the Army, U.S. Army Corps of Engineers, Washington, D.C. 20314-1000, December 1991.

[8] D. R. LYNCH AND W. G. GRAY, *A wave equation model for finite element tidal computations*, Computers and Fluids, 7 (1979), pp. 207–228.

NUMERICAL MODELING OF SHALLOW WATER FLOWS WITH WETTING AND DRYING BOUNDARIES BY A FINITE VOLUME METHOD

Clint N. Dawson*and Srinivas Chippada
Texas Institute for Computational and Applied Mathematics
University of Texas at Austin
Austin, TX 78712
clint@ticam.utexas.edu

Keywords Environmental science, Partial differential equations, Shallow water equations, Godunov method, Finite volume method

ABSTRACT

A finite volume method on unstructured meshes has been developed for solving the system of shallow water equations. The system of equations is formulated as a conservation law, and integrated over each cell. The solution is approximated on each cell by constants or linears. Numerical fluxes at cell interfaces are computed using Roe's approximate solution of the Riemann shock-tube problem. This paper outlines the method and discusses the extension of this procedure to physical problems involving wetting and drying.

INTRODUCTION.

The shallow water equations (SWE) can be used to study many physical phenomena of interest such as storm surges, tidal fluctuations, tsunami waves, forces acting on off-shore structures, and contaminant and salinity transport. Due to their practical importance, the SWE have been widely investigated and a variety of numerical methods have been developed. As in the case of Navier-Stokes equations, the coupling between the velocity field and elevation (which plays the role of density in SWE) has played an important role in the development of numerical schemes. Finite element methods based on mixed-order interpolations (e.g. King & Norton (1978)) and equal-order interpolations (e.g., Kawahara *et al.* (1982), Zienkiewicz & Ortiz (1995)) have been developed. Alternatively, numerical schemes based on equal-order interpolations and wave formulations of the SWE have also been developed (Lynch & Gray (1979), Luettich *et al.* (1991)). Numerical methods developed in the context of gas dynamics, namely, finite volume methods based on formulating Riemann problems at the cell interfaces have also been applied to the SWE (Alcrudo and Garcia-Navarro (1993), Sleigh *et al.* (1997)). The numerical method to be presented in this paper is a Godunov-type finite volume method and belongs to the last category. The basic algorithm is described in (Chippada *et al.* (1997)). Here we briefly outline the method and discuss its extension to problems with wetting and drying boundaries.

*This work supported in part by National Science Foundation grant DMA-9696177.

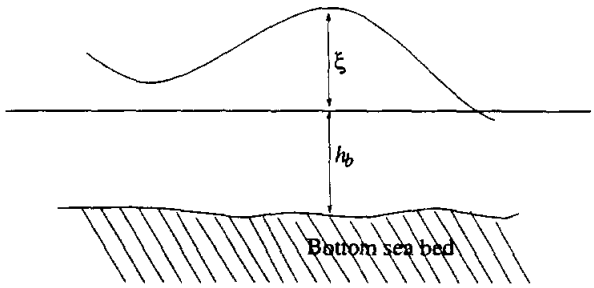

Figure 1: Definition of elevation and bathymetry

MATHEMATICAL MODEL

The system of shallow water equations are statements of conservation of mass and momentum, and are given by:

$$\frac{\partial \xi}{\partial t} + \nabla \cdot \mathbf{U} = 0, \tag{1}$$

and

$$\frac{\partial \mathbf{U}}{\partial t} + \nabla \cdot \left(\frac{\mathbf{U}\mathbf{U}}{H} \right) + \tau_{bf} \mathbf{U} + f_c \mathbf{k} \times \mathbf{U} + gH \nabla \xi = \mathbf{F}. \tag{2}$$

In the above equations, ξ represents the deflection of the air-liquid interface from the mean sea level, $H = h_b + \xi$ represents the total fluid depth, and h_b is the bathymetric depth (see Fig.1), $\mathbf{U} = \mathbf{u}H = (U, V)$ is the fluid discharge field, $\mathbf{u}$ is the depth averaged horizontal velocity field, f_c is the Coriolis parameter resulting from the earth's rotation, $\mathbf{k}$ is the local vertical vector, g is the gravitational acceleration, and τ_{bf} is the bottom friction coefficient which is usually computed using either Manning's or Chezy's friction law. In most practical applications, bottom friction dominates lateral diffusion and dispersion, and these terms are neglected in the above equations. In addition to the above described phenomena, often we need to include the effects of surface wind stress, variable atmospheric pressure and tidal potentials which are expressed through the body force $\mathbf{F}$ (Luettich *et al.*, (1991)).

On the land boundary, we have the no normal flow boundary conditions given by:

$$\mathbf{U} \cdot \nu = 0 \tag{3}$$

where ν is the unit normal. River boundaries bring in discarge into the system and are given by:

$$\mathbf{U} \cdot \nu = \hat{\mathbf{U}} \cdot \nu, \quad \text{and} \quad \xi = \hat{\xi} \tag{4}$$

where hat quantities are the incoming river values. On an open ocean boundary, usually elevation is specified as function of time:

$$\xi = \hat{\xi}. \tag{5}$$

In addition, sometimes a radiation-type boundary condition is imposed to let waves leave the domain without any reflections.

NUMERICAL MODELING

A Godunov-type finite volume method based on unstructured triangular meshes has been developed to solve the system of shallow water equations given by Eqs.1 and 2. In this method, elevation ξ and fluid discharges U and V are approximated as piecewise constants within each triangle, and numerical fluxes at cell edges are computed by solving the Riemann shock-tube problem in an approximate manner using Roe's linearization technique (Roe, 1981). This method has also been extended to a second-order accurate non-oscillatory scheme through a slope-limiter type algorithm. This numerical method is described in detail in (Chippada *et al.* (1996)). We briefly outline the scheme and then present a method for extending it to handle wetting and drying problems.

The system of SWE can be written in compact form as

$$\frac{\partial \mathbf{c}}{\partial t} + \frac{\partial \mathbf{f}_x}{\partial x} + \frac{\partial \mathbf{f}_y}{\partial y} = \mathbf{h}, \tag{6}$$

where

$$\mathbf{c} = (\xi, U, V)^T, \tag{7}$$

$$\mathbf{f}_x = \left(U, \frac{U^2}{H} - \frac{g}{2}(H^2 - h_b^2), \frac{UV}{H}\right)^T, \quad (8)$$

$$\mathbf{f}_y = \left(V, \frac{UV}{H}, \frac{V^2}{H} - \frac{g}{2}(H^2 - h_b^2)\right)^T, \quad (9)$$

and

$$\mathbf{h} = \begin{pmatrix} 0 \\ -\tau_{bf}U + f_c V + g\xi\frac{\partial h_b}{\partial x} + F_x \\ -\tau_{bf}V + f_c U + g\xi\frac{\partial h_b}{\partial y} + F_y \end{pmatrix}. \quad (10)$$

Integrating (6) over a control volume Ω_e and over a time interval $[t^n, t^{n+1}]$, we obtain

$$\int_{\Omega_e} \mathbf{c}(\cdot, t^{n+1}) d\Omega_e + \int_{t^n}^{t^{n+1}} \int_{\Gamma_e} \mathbf{f} \cdot \mathbf{n} d\Gamma_e = \int_{\Omega_e} \mathbf{c}(\cdot, t^n) d\Omega_e + \int_{t^n}^{t^{n+1}} \int_{\Omega_e} \mathbf{h} d\Omega_e.$$

Here $\mathbf{f} = (\mathbf{f}_x, \mathbf{f}_y)^T$, Γ_e is the boundary of Ω_e and $\mathbf{n}$ is the outward unit normal to Γ_e.

For triangular control volumes, the discrete equations are

$$\frac{\mathbf{c}_e^{n+1} - \mathbf{c}_e^n}{\Delta t} m(\Omega_e) + \sum_{i=1}^{3} \mathbf{f}_i^n m(\Gamma_i) = \mathbf{h}_e^n m(\Omega_e),$$

where the superscript represents the time level, c_e and h_e represent average values over the element, and $m(\Omega_e)$ and $m(\Gamma_e)$ represent the measures of Ω_e and Γ_e, respectively. In our scheme the average values are approximated by constants on each triangular element. The fluxes $\mathbf{f}_i^n$ approximate the normal flux $\mathbf{f} \cdot \mathbf{n}$ through each of the three faces of the triangle. These are calculated explicitly using the element averages of the primary variables and an approximate Riemann solver (Roe, 1981).

A higher-order variant of this algorithm can be obtained by approximating the solution over each element as a linear function. This linear is of the form

$$\mathbf{c}_L = \mathbf{c}_e + (\mathbf{x} - \mathbf{x}_e)(\delta \mathbf{c})_e, \quad (11)$$

where $\mathbf{x}_e$ is the barycenter of Ω_e. The "slope" $(\delta \mathbf{c})_e$ is calculated in a post-processing step from the average values of the cells neighboring Ω_e. The slopes are limited so as to not allow oscillations in the linear solution. The specific slope construction and limiting procedure we use are described in detail in (Chippada *et al.* 1997). Note that the linear $\mathbf{c}_L$ is mass-preserving. This linear representation is used to calculate more accurate fluxes through the edges of the boundary. The time discretization is also modified from that given above to a two-step Runge-Kutta procedure in order to increase the temporal accuracy.

WETTING AND DRYING

In problems with wetting and drying boundaries, the free surface approaches the bottom sea bed, and the fluid depth approaches zero. The shallow water equations are no longer valid in this case, and the complete 3-D Navier-Stokes equations should be solved. This of course is nontrivial, and hence there has been a great deal of effort in modifying shallow water simulators to handle problems with wetting and drying boundaries. The aim is to modify the numerical scheme so that it will not break down near contact points and at the same time models the movement of the water front with reasonable accuracy. Fortunately, in the context of the finite volume method described above, this can be done quite easily.

Sleigh *et al.* (1997), Zhao *et al.* (1994) and a few others have already done some work on extending finite volume schemes to the case of wetting/drying boundaries. Their idea is to check the fluid depth in a cell, and if it is less than a cut-off depth H_0, to declare it as a dry cell and remove it from the computations. This basic procedure can be further refined by including partially wet cells in addition to wet and dry cells. Furthermore, the equations are reformulated in a partially wet cell by neglecting the inertial terms. Sleigh

et al. (1997) consider only mass flux and set momentum fluxes to zero in a partially wet cell.

In our numerical scheme, we use a slightly different approach. We don't allow the cell to dry up completely and always maintain a thin layer of fluid. Thus if the fluid depth falls below a cut-off depth H_0, the fluid depth is reset to H_0 and the flow velocities are set to zero within that element. In this way, there is no need to keep track of wet and dry cells. Flux calculations are done over all cell edges and the fluid depth and fluid velocities are updated in all cells. As will be clear from the results to be presented in the next section, this simple procedure works very well and gives accurate results for a dam break problem, where an analytical solution is known.

RESULTS

A one-dimensional dam break problem is solved first. The dam breaks at time $t = 0$, and the fluid that is initially at rest upstream of the dam rushes downstream, which is assumed to be initially dry. The bottom of the river bed is assumed to be friction-less, and all other phenomena such as Coriolis forces, wind stress and atmospheric stress are not considered. This problem has an analytical solution (Toro, 1992). The numerical solution obtained is shown in Fig.2, and compared against the analytical solution in Fig.3. The mesh size $\Delta x = 0.1m$, and the time step size $\Delta t = 0.01s$. Two different cut-off depths of $H_0 = 1.0^{-3}m$ and $H_0 = 1.0^{-6}m$ have been used to flag a cell as a wet or a dry cell. Some differences between the numerical solution and the exact solution occur at the head and the foot of the wave front. At the top of the wave front the differences are due to numerical damping. At the foot of the front, the differences are due to our treatment of the wetting/drying boundary. However, the errors due to ad hoc cut-off lengths are not significant and the numerical solution is seen to be only weakly influenced by the cut-off depth.

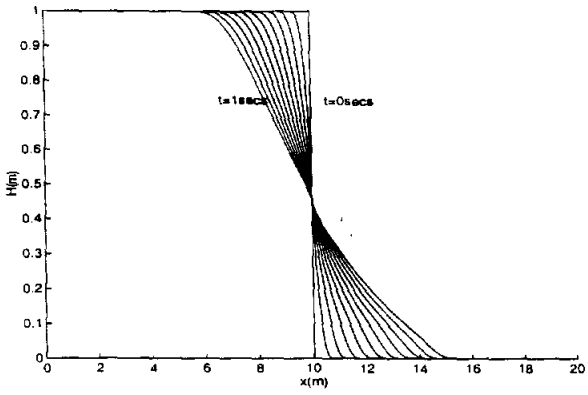

Figure 2: Numerical solution of the 1-D dam break problem.

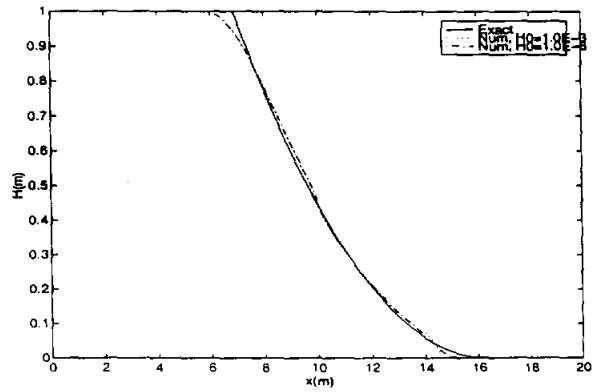

Figure 3: Comparison of 1-D numerical solutions with analytical solution.

To test our 2-D unstructured numerical algorithm, the same 1-D dam break problem is solved as a two-dimensional problem, with the fluid being confined by solid free-slip walls on either side. The numerical mesh used, fluid depth contours at the end of time $t = 1$ second, and comparison of the fluid depth at the centerline with analytical solution are shown in Figs.4- 6. A numerical cut-off depth of $H_0 = 10^{-3}m$ is used in this simulation. Again, we find very good agreement between the numerical solution and the exact solution.

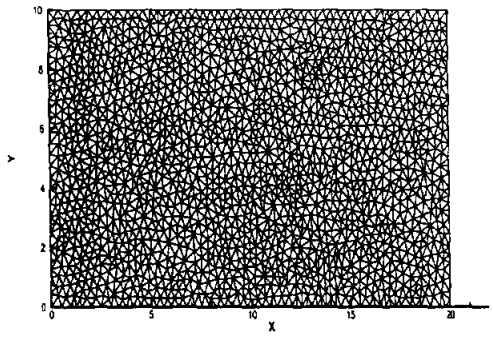

Figure 4: Numerical mesh used in solving 1-D dam break problem in a 2-D domain.

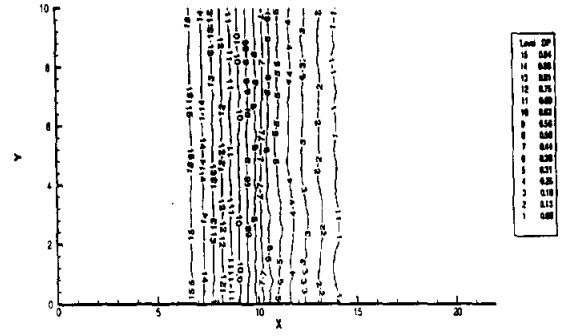

Figure 5: Fluid depth contours at the end of 1s for the dam break problem.

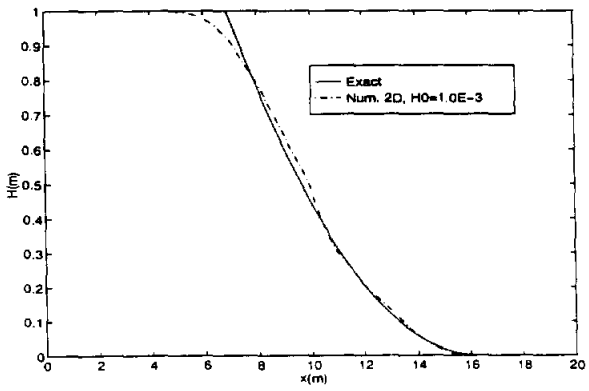

Figure 6: Comparison of 2-D numerical solution with analytical solution for fluid depth at the end of 1s.

CONCLUSIONS

A Godunov-type finite volume method based on unstructured triangular meshes and Roe's approximate Riemann solver has been developed. This numerical procedure has been shown to model wetting and drying problems in a simple and accurate manner. Application of this procedure to the study of storm surges and flood plains is in progress.

REFERENCES

1. Alcrudo, F., and Garcia-Navarro, P., 1993. "A high-resolution Godunov-type scheme in finite volumes for the 2D shallow-water equations," *Int. J. Num. Meth. Fluids 16*:489–505.

2. Chippada, S., Dawson, C. N., Martinez, M. L., and Wheeler, M. F., "A Godunov-type finite volume method for system of shallow water equations," *Computer Methods in Applied Mechanics and Engineering*, to appear.

3. Kawahara, M., Hirano, H., Tsuhora, K., and Iwagaki, K., 1982, "Selective lumping finite element method for shallow water equations," *Int. J. Num. Meth. Engg. 2*:99-112.

4. King, I.P., and Norton, W.R., 1978. "Recent application of RMA's finite element models for two-dimensional hydrodynamics and water quality," in Finite Elements in Water Resources II, C.A. Brebbia, W.G.Gray, and G.F.Pinder, eds., Pentech Press, London.

5. LeVeque, R. J., 1992, *Numerical Methods for Conservation Laws*, Birkhauser Verlag.

6. Luettich, Jr., R. A., Westerink, J. J., and Scheffner, N. W., 1991. "ADCIRC:

An Advanced Three-Dimensional Circulation Model for Shelves, Coasts and Estuaries," Report 1, U.S. Army Corps of Engineers, Washington, D.C. 20314-1000, December 1991.

7. Lynch, D.R., and Gray, W., 1979. "A wave equation model for finite element tidal computations," *Comput. Fluids* 7:207–228.

8. Roe, P. L., 1981. "Approximate Riemann solvers, parameter vectors, and difference schemes," *J. Comput. Phys.* *43*:357–372.

9. Sleigh, P.A., Berzins, M., Gaskell, P. H., and Wright, N. G., 1997. "An unstructured finite-volume algorithm for predicting flow in rivers and estuaries," preprint.

10. Zhao, D. H., Shen, H. W., Tabois, G. Q., Tan, W. Y., and Lai, J. S., 1994. "Finite-volume 2-dimensional unsteady-flow model for river basins," *Journal of Hydraulic Engineering-ASCE* *120*:863–883.

11. Zienkiewicz, O.C., and Ortiz, P., 1995. "A split-characteristic based finite element model for the shallow water equations," *Int. J. Num. Meth. Fluids* *20*:1061–1080.

Reprinted from

Computer methods in applied mechanics and engineering

Comput. Methods Appl. Mech. Engrg. 157 (1998) 1–10

A projection method for constructing a mass conservative velocity field[1]

S. Chippada*, C.N. Dawson, M.L. Martínez, M.F. Wheeler

Center for Subsurface Modeling, Texas Institute for Computational and Applied Mathematics, University of Texas, Austin, TX 78712, USA

Received 22 January 1998

ELSEVIER

COMPUTER METHODS IN APPLIED MECHANICS AND ENGINEERING
EDITORS: J.H. ARGYRIS, STUTTGART and LONDON
T.J.R. HUGHES, STANFORD, CA
J.T. ODEN, AUSTIN, TX

W. PRAGER
Founding Editor
(deceased 1980)

International Standard Serial Number 0045-7825

Printed in The Netherlands

ELSEVIER

Comput. Methods Appl. Mech. Engrg. 157 (1998) 1–10

Computer methods in applied mechanics and engineering

A projection method for constructing a mass conservative velocity field[1]

S. Chippada*, C.N. Dawson, M.L. Martínez, M.F. Wheeler

Center for Subsurface Modeling, Texas Institute for Computational and Applied Mathematics, University of Texas, Austin, TX 78712, USA

Received 22 January 1998

Abstract

In the numerical modeling of fluid flow and transport problems, the velocity field frequently needs to be projected from one finite dimensional space into another. In certain applications, especially those involving modeling of multi-species transport, the new projected velocity field should be accurate as well as locally mass conservative.

In this paper, a velocity projection method has been developed that is both accurate and mass conservative element-by-element on the projected grid. The velocity correction is expressed as gradient of a scalar pressure field, and the resultant Poisson equation is solved using a mixed/hybrid finite element method and lowest-order Raviart–Thomas spaces. The conservative projection method is applied to the system of shallow water equations and a theoretical error estimate is derived. © 1998 Elsevier Science S.A.

1. Introduction

In the numerical modeling of fluid flow and transport problems, the computed velocity field frequently needs to be projected from one finite dimensional subspace into another, possibly to satisfy some constraint or because the underlying mesh has changed. For example, in Lagrangian-based numerical modeling of free boundary problems, to avoid mesh distortions the numerical mesh is regenerated once every few time steps, and in such situations the velocity field has to be projected from the old grid onto the new grid. Other important applications where the velocity field may need to be projected are in the modeling of environmental surface and subsurface flow and transport problems. In these problems, the flow and transport equations arise from conservation of mass (plus some additional equations such as Darcy's Law or the Navier–Stokes equations). The flow and multi-species transport are often solved separately using completely different numerical methods and grids due to differences in length and time scales of the phenomena involved. For accurate transport, it is desirable for the velocities to be locally conservative on the transport grid. This can be accomplished through the projection algorithm described below.

A particular example on which we will focus is the modeling of surface flow. Here the flow model is described by the shallow water equations. The ADCIRC (an advanced circulation model for shelves, coasts and estuaries) [7,8] and RMA codes [5] are examples of widely used shallow water hydrodynamics models. Both models are based on Galerkin-type finite element methods and unstructured triangular grids. The velocities computed with these models can serve as input to a multi-species transport model. For example, the

* Corresponding author.

[1] This paper is dedicated to J. Tinsley Oden on the occasion of his 60th birthday.

PII S0045-7825(97)00062-0

CE-QUAL-ICM [2] simulator is a widely used water quality model. It uses unstructured quadrilateral grids and finite volume type discretization. All of these codes are utilized by US Army Corps of Engineers at the Waterways Experiment Station in Vicksburg, Mississippi, and other state and federal agencies in modeling environmental quality of shallow water systems. Therefore, there is a need to couple these hydrodynamic and water quality models and to perform a projection to produce a locally conservative velocity field on the transport grid.

In this paper we present an approach which we call the *conservative velocity projection method*, which projects a computed velocity field from one finite dimensional space into another in an accurate and element-by-element mass conservative manner. In particular, we will focus on a projection algorithm based on the mixed/hybrid finite element method. This method is well-suited for computing locally conservative velocity fields.

In Section 2, the mathematical aspects of hydrodynamics and environmental modeling are briefly discussed. The conservative projection method and the mixed/hybrid finite element method are outlined in Section 3. An error estimate for the accuracy of the projected velocity field is derived in Section 4. The application of the projection method to the shallow water equations modeled using the ADCIRC code is presented in Section 5. Finally, in Section 6, we conclude with some remarks and future research possibilities.

2. Flow and transport modeling

The most general form of the conservation of mass equation is given by

$$\frac{\partial \rho}{\partial t} + \nabla \cdot \boldsymbol{U} = q\,. \tag{1}$$

In the above equation, ρ is the the fluid density, $\boldsymbol{u}$ is the velocity vector field, $\boldsymbol{U} = \rho \boldsymbol{u}$, ∇ is the spatial gradient operator and q represents the sources and sinks that may be present in the flow domain. In most hydrodynamics situations the fluid flow is incompressible and the mass conservation equations simplifies to

$$\nabla \cdot \boldsymbol{u} = q\,. \tag{2}$$

We present the projection method for a fluid flow system with conservation of mass of the form given by Eq. (1), but the procedure and analysis carries forward in a straightforward manner to the case of incompressible flows also. Further, in the case of shallow water systems, even though the fluid flow is governed by the 3-D incompressible Navier–Stokes equations, after depth-averaging we obtain a mathematical system which is compressible in nature with conservation of mass equation of the form given by Eq. (1) and the fluid depth H playing the role of density.

The fluid flow mathematical model typically consists of a mass conservation equation given by either Eqs. (1) or (2) and a momentum conservation law. Several forms of momentum conservation laws are used depending on the flow situations. In high-speed aerodynamic flows compressible Navier–Stokes equations are used whereas in the case of low speed hydraulic flows the incompressible Navier–Stokes equations are solved. In the case of flow through porous media the velocity field is determined using Darcy's law. In certain flow problems the energy equation and an equation of state may also have to be solved simultaneously along with the mass and momentum equations. The actual form of the fluid flow model itself is not important since in this paper we are only interested in post-processing a given fluid flow field so that it is locally mass-conservative on the same grid or on an entirely new grid. As proof-of-concept, we apply the conservative velocity projection method to the fluid flow governed by the system of shallow water equations and this hydrodynamics model is described in detail in Section 5.

We assume that we have a hydrodynamics model governing the fluid flow consisting of a mass conservation law (Eq. (1)) and a momentum conservation law and any other equations that may be necessary to compute the flow field. This system is numerically solved using any of the existing finite difference, finite element and finite volume type numerical schemes.

The multi-species transport model consists of a system of advection–diffusion-reaction type transport equations of the following form:

$$\frac{\partial(\rho c_i)}{\partial t} + \nabla\cdot(\rho \boldsymbol{u} c_i) = \nabla\cdot(D_i \nabla c_i) + q c_i - R_i, \quad i = 1, \ldots, N, \tag{3}$$

where c_i is the concentration per unit mass of species i, R_i is a reaction-type source function and D_i is the diffusion coefficient. The primary influence of the flow field is in the advective transport of the concentration species. In case of turbulent fluid flows the velocity field can also influence the diffusion coefficient D_i. Here, we are assuming passive scalar transport and that the concentration field does not affect the fluid flow. If this is not the case then we need to solve the hydrodynamics and concentration equations together preferably on the same grids.

In the numerical solution of the concentration equations it is important that the velocity field be mass conservative cell-by-cell. This can be seen more clearly if we rewrite the transport equation (Eq. (3)) in the following way:

$$\rho\left(\frac{\partial c_i}{\partial t} + \boldsymbol{u}\cdot\nabla c_i - \frac{1}{\rho}\nabla\cdot(D_i\nabla c_i) - \frac{1}{\rho}R_i\right) + c_i\left(\frac{\partial \rho}{\partial t} + \nabla\cdot(\rho \boldsymbol{u}) - q\right) = 0. \tag{4}$$

The mass conservation equation is present in the species transport equation (Eq. (3)), and if we do not have local mass conservation it amounts to adding spurious sources and sinks. This could give rise to numerical instabilities, especially if we are interested in integrating the equations over long periods of time. Also, in some applications the concentrations are very small (of the order of 10^{-6}) and small errors in mass conservation can have significant influence on the accuracy and stability of the system. Thus, it is important for the velocity field to be cell-by-cell mass conservative in the multi-species transport studies.

3. Conservative projection formulation

Let $\Omega \in R^n$, $n = 2$ or 3, be the physical domain and $\partial\Omega$ the external boundary of this domain. Further, let $\partial\Omega_1$ be the boundary on which we have Dirichlet boundary conditions on the normal velocity expressed as

$$\boldsymbol{U}\cdot\boldsymbol{\nu} = g \quad \text{on } \partial\Omega_1, \tag{5}$$

where $\boldsymbol{\nu}$ is the outward pointing unit normal vector at the boundary. Let h^o be the mesh parameter of the old grid and h^n be the mesh parameter of the new grid. Further, let $\bar{V}_{h^o}$ and $\bar{V}_{h^n}$ be finite dimensional subspaces corresponding to the old and new meshes. Given $U_{h^o} \in \bar{V}_{h^o}$ the problem is to find $U_{h^n} \in V_{h^n}$ such that U_{h^n} is a close approximation of U_{h^o} and that U_{h^n} 'satisfies' the mass conservation law given by

$$\nabla\cdot U_{h^n} = q - \frac{\partial\rho}{\partial t} = f \quad \text{in } \Omega,$$

and (6)

$$U_{h^n}\cdot\boldsymbol{\nu} = g \qquad \text{on } \partial\Omega_1.$$

The new velocity U_{h^n} is expressed in terms of the old velocity U_{h^o} in the following manner:

$$U_{h^n} = \mathscr{P}_{h^n} U_{h^o} + \Gamma_{h^n} \in V_{h^n}, \tag{7}$$

where $\mathscr{P}_{h^n} U_{h^o}$ is the $\mathscr{L}^2$ projection of the old velocity U_{h^o} into V_{h^n} and $\Gamma_{h^n} \in V_{h^n}$ is the velocity correction which we need to compute. Substituting Eq. (7) into Eq. (6) we obtain the following boundary value problem:

$$\nabla\cdot\Gamma_{h^n} = f - \nabla\cdot\mathscr{P}_{h^n}U_{h^o} = \tilde{f} \quad \text{in } \Omega,$$

and (8)

$$\Gamma_{h^n}\cdot\boldsymbol{\nu} = g - \mathscr{P}_{h^n}U_{h^o}\cdot\boldsymbol{\nu} = \tilde{g} \quad \text{on } \partial\Omega_1.$$

Further, we express Γ_{h^n} as the gradient of a scalar function in the following manner:

$$\Gamma_{h^n} = -\nabla\phi_{h^n}. \tag{9}$$

The scalar variable ϕ_{h^n} can be thought of as a pseudo-pressure. This type of representation implies that the

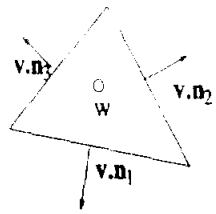

Fig. 1. Piece-wise approximations on a triangular element using lowest-order Raviart–Thomas spaces.

vorticity of the new velocity field U_{h^n} is same as that of the old velocity field $\mathscr{P}_{h^n}U_{h^o}$ and the velocity correction Γ_{h^n} helps us obtain local mass conservation without changing the vorticity of the velocity field. Substituting Eq. (9) into Eq. (8) we obtain the following elliptic problem:

$$\begin{aligned} &-\Delta\phi_{h^n} = \tilde{f} && \text{on } \Omega\,, \\ \text{and}\quad &-\nabla\phi_{h^n}\cdot = \tilde{g} && \text{on } \partial\Omega_1\,, \\ &\phi_{h^n} = 0 && \text{on } \partial\Omega/\partial\Omega_1\,. \end{aligned} \tag{10}$$

The elliptic problem given by Eq. (10) is solved using the mixed/hybrid finite element method which approximates both fluxes (Γ) and pressures (ϕ). In addition, the fluxes $\Gamma\cdot\nu = -\nabla\phi\cdot\nu$ are continuous across the edges and the resulting numerical solution satisfies mass conservation cell-by-cell. The mixed/hybrid finite element approximation of the elliptic problem (Eq. (10)) together with velocity relations (Eqs. (7) and (9)) represent the *conservative velocity projection formulation*.

On the new grid, the elliptic problem is approximated using triangular elements and lowest-order Raviart–Thomas spaces which are written as follows for a given triangular element E (see Fig. 1):

$$W_{h^n}(E) = \{a \in R \text{ on } E\}\,, \tag{11}$$

and

$$V_{h^n}(E) = \begin{pmatrix} \alpha + \beta x \\ \gamma + \beta y \end{pmatrix}; \qquad \alpha, \beta, \gamma \in R\,, \quad (x, y) \in E\,. \tag{12}$$

The finite dimensional scalar and vector spaces on the new grid are defined as

$$W_{h^n} = \{w \in \mathscr{L}^2(\Omega)\colon w|_E \in W_{h^n}(E) \forall\, E\} \tag{13}$$

$$\boldsymbol{V}_{h^n} = \{\boldsymbol{v} \in \mathscr{L}^2(\Omega)\colon \boldsymbol{v}|_E \in \boldsymbol{v}_{h^n}(E) \forall\, E\} \tag{14}$$

In the mixed/hybrid finite element method the second-order elliptic problem is written as a first-order system and we compute $\Gamma_{h^n}, \phi_{h^n}) \in (V_{h^n}, W_{h^n})$ from

$$\begin{aligned} &(\Gamma_{h^n}, \boldsymbol{v}_{h^n}) - (\phi_{h^n}, \nabla\cdot\boldsymbol{v}_{h^n}) = 0 && \forall\, \boldsymbol{v}_{h^n} \in V_{h^n} \\ &(\nabla\cdot\Gamma_{h^n}, w_{h^n}) = (\tilde{f}, w_{h^n}) && \forall\, w_{h^n} \in W_{h^n} \\ &\langle \Gamma_{h^n}\cdot\nu, \boldsymbol{v}_{h^n}\cdot\nu\rangle = \langle \tilde{g}, \boldsymbol{v}_{h^n}\cdot\nu\rangle && \forall\, \boldsymbol{v}_{h^n} \in V_{h^n} \end{aligned} \tag{15}$$

In the above weak formulation, $(\cdot,\cdot)$, and $\langle\cdot,\cdot\rangle$ are the the usual inner products on the domain Ω and the boundary $\partial\Omega$, respectively. We refer the reader to Raviart and Thomas [10] and Brezzi and Fortin [1] for more information on the mixed/hybrid finite element method and their implementation details.

4. Theoretical error estimate

The $\mathscr{L}^2$ projection of U_{h^o} into V_{h^n} is defined by

$$((U_{h^o} - \mathscr{P}_{h^n}U_{h^o}), \boldsymbol{v}_{h^n}) = 0\,, \quad \forall\, \boldsymbol{v}_{h^n} \in V_{h^n}\,.$$

Also, the Π projection of U into V_{h^n} is defined as

$$(\nabla \cdot (U - \Pi_{h^n} U), w_{h^n}) = 0, \quad \forall w_{h^n} \in W_{h^n}$$

THEOREM 4.1. Given U_{h^n}, U_{h^o}, $\exists$ a constant C independent of h^n, h^o, U such that

$$\|U_{h^n} - U\| \leq C(\|\Pi_{h^n} U - U\| + \|U_{h^o} - U\|). \tag{16}$$

PROOF. First, write Eq. (7) in weak form to get

$$(U_{h^n}, v_{h^n}) = (\mathcal{P}_{h^n} U_{h^o}, v_{h^n}) + (\Gamma_{h^n}, v_{h^n}), \quad \in \forall\, v_{h^n} \in V_{h^n}. \tag{17}$$

Subtract (U, v_{h^n}) from both sides of Eq. (17) and use the definition of the $\mathcal{L}^2$ projection to get

$$(U_{h^n} - U, v_{h^n}) = (U_{h^o} - U, v_{h^n}) + (\Gamma_{h^n}, v_{h^n}), \quad \forall\, v_{h^n} \in V_{h^n}. \tag{18}$$

By choosing $v_{h^n} = U_{h^n} - \Pi_{h^n} U$, we can reduce to zero the second term in the right-hand side of Eq. (18). This is accomplished by using our chosen test function in the first relation of Eq. (15), together with the definition of the Π_{h^n} projection and the fact that the mass conservation equation is satisfied by both the true velocity U and the new velocity U_{h^n}.

Finally, manipulate

$$(U_{h^n} - U, (U_{h^n} - U) - (\Pi_{h^n} U - U)) = (U_{h^o} - U, (U_{h^n} - U) - (\Pi_{h^n} U - U))$$

using Cauchy–Schwartz and the arithmetic-geometric-mean inequality,

$$ab \leq \frac{1}{4\epsilon} a^2 + \epsilon b^2, \quad \epsilon > 0,$$

to obtain the result of the theorem. □

The elegance of the estimate comes from the observation that it reduces to an approximation theory question given an estimate for the difference between U_{h^o} and the true velocity U.

For example, using the lowest-order Raviart–Thomas space in computing U_{h^n} [10,1] and using, say, the ADCIRC model to compute U_{h^o} [4], then $\|U_{h^n} - U\| \leq Ch$.

5. Application: Shallow water equations

The projection formulation developed in Section 3 is applied to the system of shallow water equations. Shallow water equations (SWE) are obtained through the vertical integration of the 3-D incompressible Navier–Stokes along with assumptions of hydrostatic pressure and vertically uniform velocity profiles [11]. Due to the assumptions made in their derivation, SWE are valid only for flow systems with horizontal length scales much larger compared to the fluid depth. A typical shallow water system is shown in Fig. 2. The conservation of mass in the system of shallow water equations is given by

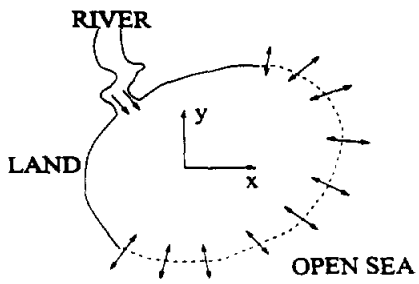

Fig. 2. A typical shallow water system.

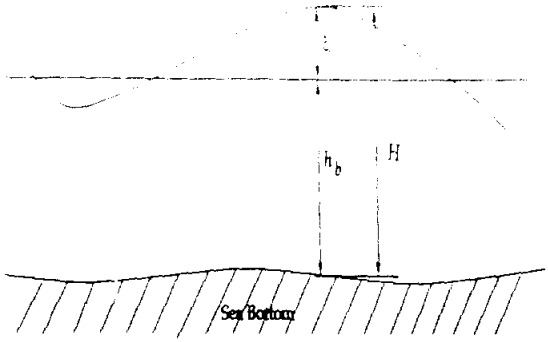

Fig. 3. Definition of ξ, h_b and H.

$$\mathscr{L} \equiv \frac{\partial \xi}{\partial t} + \nabla \cdot (\boldsymbol{u} H) = 0 . \tag{19}$$

The non-conservative form of the momentum equation is as follows:

$$\mathscr{M} \equiv \frac{\partial \boldsymbol{u}}{\partial t} + \boldsymbol{u} \cdot \nabla \boldsymbol{u} + g \nabla \xi - \frac{1}{H} \nabla \cdot [H \boldsymbol{\sigma}] + \tau_{bf} \boldsymbol{u} + f_c \boldsymbol{k} \times \boldsymbol{u} - f_b = 0 . \tag{20}$$

In the above system, ξ is the deflection of the air–water interface from the mean sea level (see Fig. 3), $H = \xi + h_b$ is the total fluid depth and h_b is the bathymetric depth. The velocity field is denoted by $\boldsymbol{u}$ and is the mean velocity across the vertical. $\boldsymbol{U} = \boldsymbol{u}H$ is the total flow rate (discharge) and τ_{bf} and f_c are, respectively the bottom friction and Coriolis acceleration coefficients; $\boldsymbol{\sigma}$ is the viscous stress tensor and is neglected in most applications since the bottom friction terms dominate the lateral diffusion and dispersion. Several types of body forces act on the system including the wind stress, atmospheric pressure gradient and tidal potential forces and

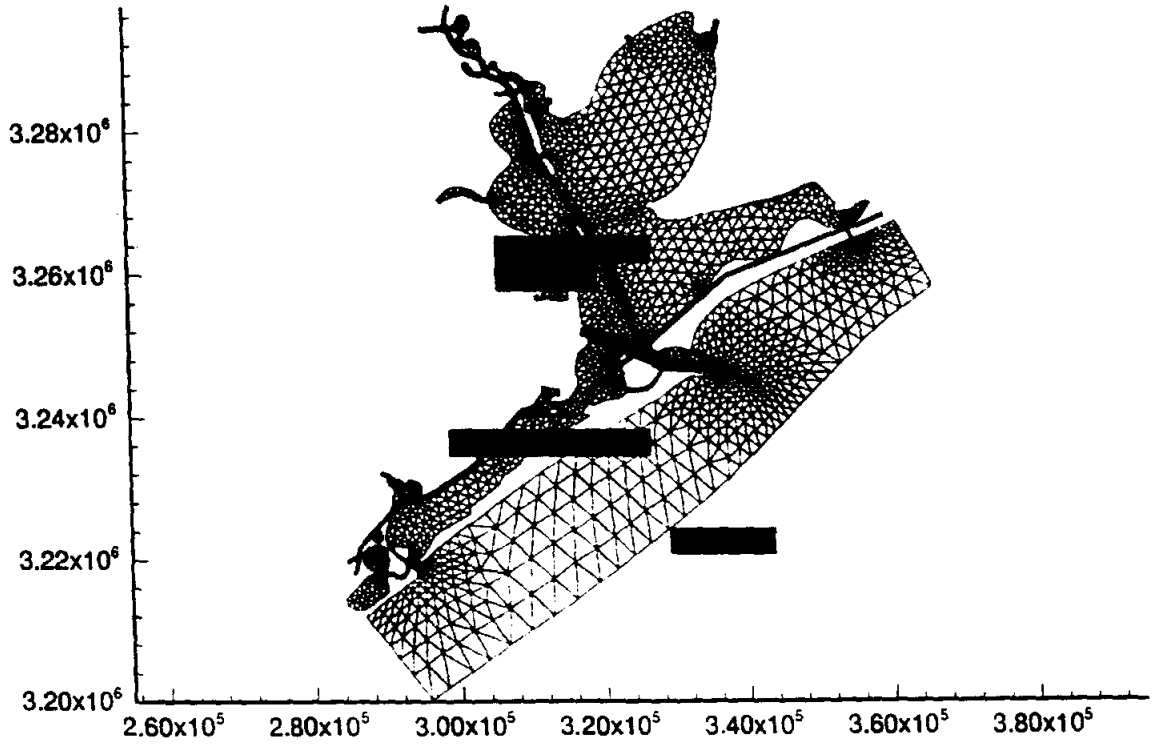

Fig. 4. Galveston Bay: numerical mesh. Lengths shown are in meters.

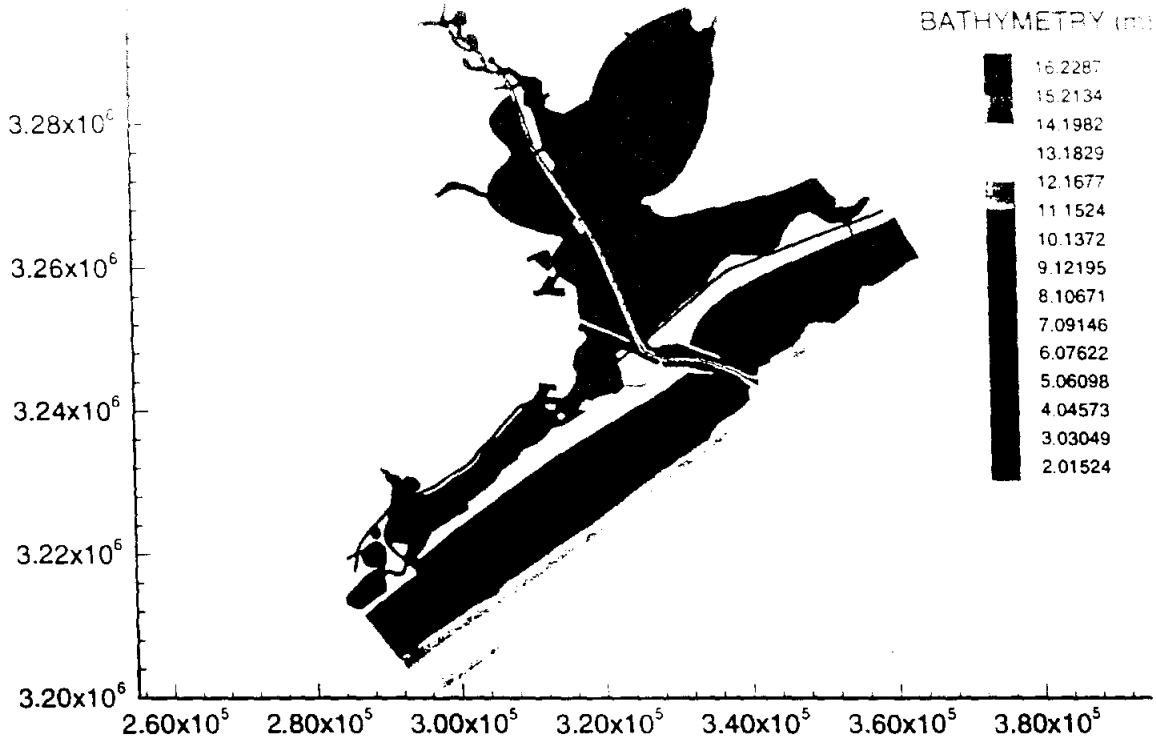

Fig. 5. Galveston Bay: bathymetry. Lengths shown are in meters.

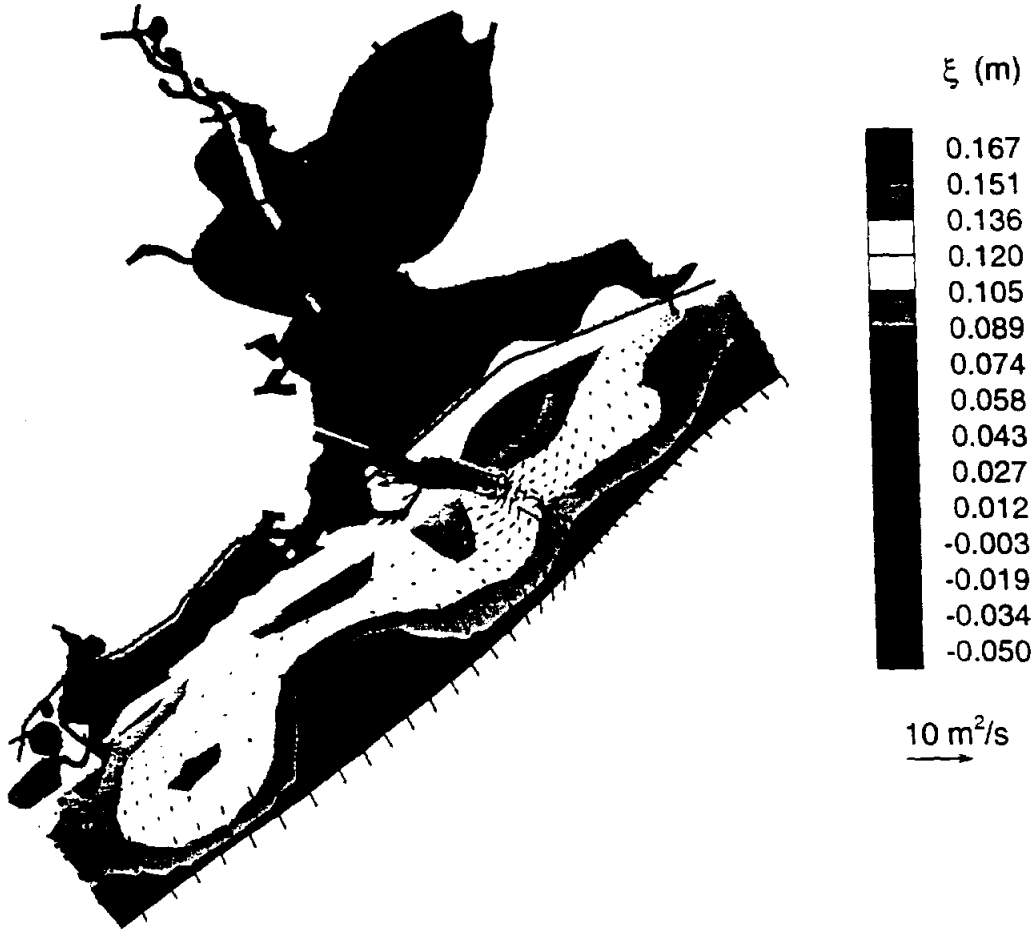

Fig. 6. Galveston Bay: ADCIRC solution at-the end of 12 days.

all of these are lumped into the generic body force term f_b. The conservative form of the momentum equation can be derived from Eqs. (19) and (20) in the following manner

$$\mathcal{M}_c \equiv H\mathcal{M} + u\mathcal{L} = 0 \tag{21}$$

A variety of numerical methods have been developed to solve the system of shallow water equations. Due to the strong coupling between the velocity and elevation fields, if the numerical method is not chosen properly, we could run into the problem of spurious spatial oscillations. Gray et al. [7,8] have developed over the years a numerical procedure (code) called ADCIRC. They replace the first-order mass conservation equation (Eq. (19)) with a second-order generalized wave continuity equation (GWCE) which is given by

$$\mathcal{G} \equiv \frac{\partial L}{\partial t} - \nabla \cdot \mathcal{M}_c + \tau_0 \mathcal{L} = 0 \tag{22}$$

The resulting form of the GWCE is

$$\frac{\partial^2 \xi}{\partial t^2} + \tau_0 \frac{\partial \xi}{\partial t} + \nabla \cdot [(\tau_0 - \tau_{bf})\boldsymbol{Hu}] - \nabla \cdot [\nabla \cdot (\boldsymbol{Huu}) + Hf_c \boldsymbol{k} \times \boldsymbol{u} + gH\nabla\xi - \nabla \cdot [H\boldsymbol{\sigma}] - Hf_b] = 0 \tag{23}$$

In the above equation, τ_0 is a numerical parameter which is chosen based on stability and accuracy criteria and is usually 1–10 times the bottom friction coefficient τ_{bf} [6]. The GWCE (Eq. (23)) along with the non-conservative momentum equation (Eq. (20)) is solved using the Galerkin finite element method and linear triangular elements. The main advantage of this method is that it lets us choose the same approximating spaces for both the velocities and pressure without giving rise to spurious spatial oscillations. Thus, this approach is

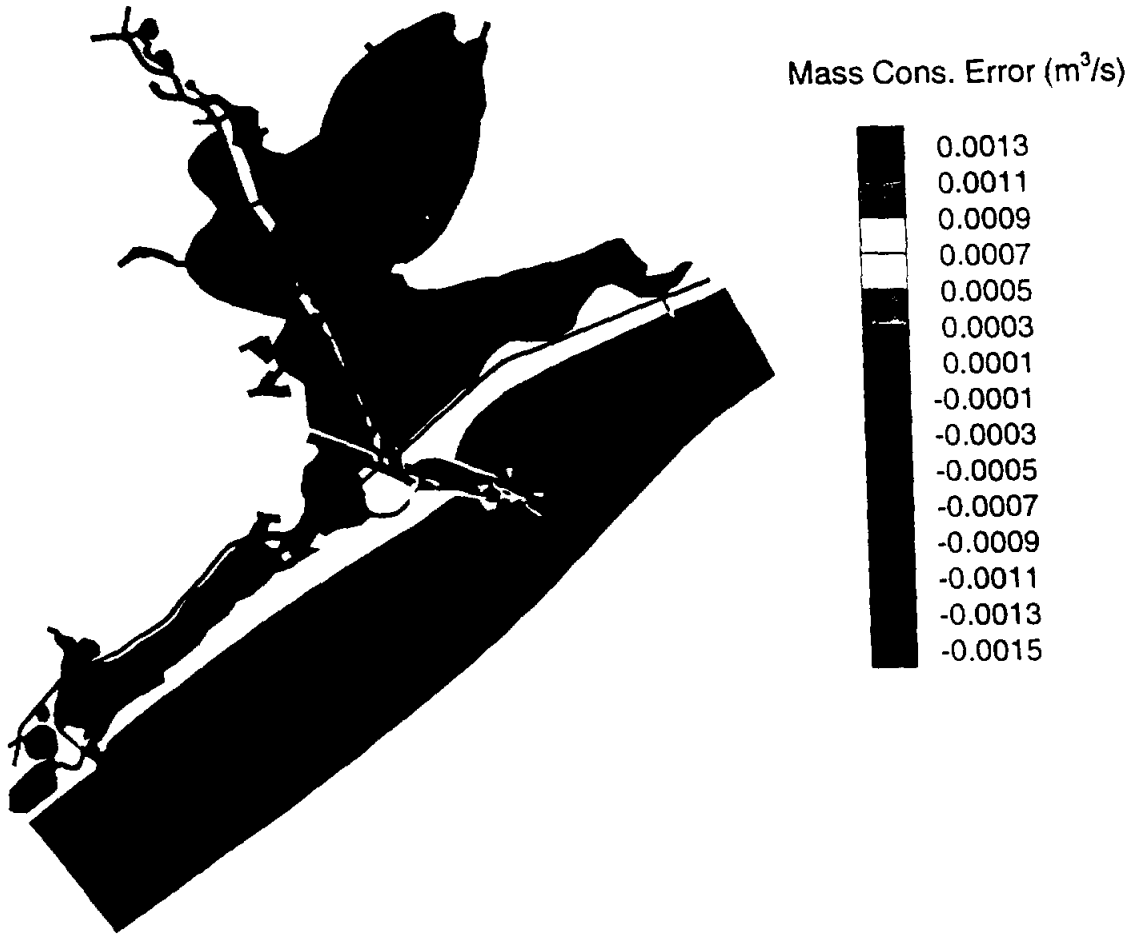

Fig. 7. Galveston Bay: local mass conservation error.

6. Concluding remarks and future work

A conservative velocity projection scheme that projects the velocity field from one grid onto another in an accurate and locally mass conservative manner has been defined. A theoretical error estimate of the conservative projection formulation has been derived and numerical results pertaining to the system of shallow water equations have been presented. The procedure proposed in this paper is very general and extends readily to 3-D and other general elements. Another advantage of this procedure is that it can be applied only in regions of large mass conservation errors thus giving great computational efficiency.

In the future, we are looking at coupling 3-D ADCIRC velocities with CE-QUAL-ICM. We also plan to investigate the application of this approach to non-matching grids.

Acknowledgments

The authors thank J.J. Westerink for sharing the ADCIRC code and data sets. This work was partially funded by the National Science Foundation, Project No. DMS-9408151.

References

[1] F. Brezzi and M. Fortin, Mixed and Hybrid Finite Element Methods (Springer-Verlag, New York, 1991).

[2] C.F. Cerco and T. Cole, User's Guide to the CE-QUAL-ICM Three-dimensional eutrophication model, Release Version 1.0, Technical Report EL-95-15, U.S. Army Engineer Waterways Experiment Station, Vicksburg, MS, 1995.

[3] R.S. Chapman, T. Gerald and M.S. Dortch, Development of unstructured grid linkage methodology and software for CE-QUAL-ICM, Private communication.

[4] S. Chippada, C.N. Dawson, M.L. Martínez and M.F. Wheeler, Finite element approximations to the system of shallow water equations, Part I: Continuous time a priori error estimates, SIAM J. Numer. Anal., to appear.

[5] I.P. King and W.R. Norton, Recent application of RMA's finite element models for two-dimensional hydrodynamics and water quality, in: C.A. Brebbia, W.G. Gray and G.F. Pinder, eds., Finite Elements in Water Resources II (Pentech Press, London, 1978).

[6] R. Kolar, W.G. Gray, and J.J. Westerink, Boundary conditions in shallow water models—An alternative implementation for finite element codes, Int. J. Numer. Methods Fluids 22(7) (1996) 603–618.

[7] D.R. Lynch and W. Gray, A wave equation model for finite element tidal computations, Comput. Fluids 7 (1979) 207–228.

[8] R.A. Luettich Jr., J.J. Westerink and N.W. Scheffner, ADCIRC: An Advanced Three-dimensional circulation model for shelves, coasts and estuaries, Report 1, U.S. Army Corps of Engineers, Washington, D.C. 20314-1000, December 1991.

[9] W.R. Norton, I.P. King and G.T. Orlob, A finite element model for lower granite reservoir, Water Resource Engineers, Inc., Walnut Creek, CA.

[10] R.A. Raviart and J.M. Thomas, A mixed finite element method for 2nd order elliptic problems, Mathematical Aspects of the Finite Element Method, Lecture Notes in Mathematics, 606 (Springer-Verlag, New York, 1977) 292–315.

[11] T. Weiyan, Shallow Water Hydrodynamics (Elsevier Oceanography Series, 55, Elsevier, Amsterdam) 1992.

INFORMATION FOR CONTRIBUTORS

Manuscripts should be sent in triplicate to one of the Editors. All manuscripts will be refereed. Manuscripts should preferably be in English. They should be typewritten, double-spaced, first copies (or clear Xerox copies thereof) with a wide margin. Abstracts, footnotes and lists of references should also be double-spaced. All pages should be numbered (also those containing references, tables and figure captions). Upon acceptance of an article, author(s) will be asked to transfer copyright of the article to the publisher. This transfer will ensure the widest possible dissemination of information.

Abstracts
The text of a paper should be preceded by a summary in English. This should be short, but should mention all essential points of the paper.

Figures and tables
The drawings for the figures must be originals, drawn in black India ink in large size and carefully lettered, or printed on a high-quality laser printer. The lettering as well as the details should have proportionate dimensions, so as not to become illegible or unclear after the usual reduction by the printers; in general, the figures should be designed for a reduction factor of two or three. Mathematical symbols should be entered in italics, where appropriate. Each figure should have a number and a caption; the captions should be collected on a separate sheet. The appropriate place of a figure should be indicated in the margin. Tables should be typed on separate sheets. Each table should have a number and a title. The appropriate places for the insertion of tables should be indicated in the margin. Colour illustrations can be included and will be printed in colour at no charge if, in the opinion of the Editors, the colour is essential. If this is not the case, the figures will be printed in black and white unless the author is prepared to pay the extra costs arising from colour reproduction.

Formulae
Displayed formulae should be numbered and typed or clearly written by hand. Symbols should be identified in the margin, where they occur for the first time.

References
In the text, reference to other parts of the paper should be made by section (or equation) number, but not by page number. References should be listed on a separate sheet in the order in which they appear in the text.

COMPLETE INSTRUCTIONS TO AUTHORS are published in every last issue of a volume, and copies can also be obtained from the Editors and the Publisher, Elsevier Science B.V., P.O. Box 1991, 1000 BZ Amsterdam, The Netherlands.

Instructions for LaTeX manuscripts
The LaTeX files of papers that have been accepted for publication may be sent to the Publisher by e-mail or on a diskette (3.5" or 5.25" MS-DOS). If the file is suitable, proofs will be produced without rekeying the text. The article should be encoded in Elsevier-LaTeX, standard LaTeX, or AMS-LaTeX (in document style "article"). The Elsevier-LaTeX package, together with instructions on how to prepare a file, is available from the Publisher. This package can also be obtained through the Elsevier WWW home page (http://www.elsevier.nl/), or using anonymous FTP from the Comprehensive TeX Archive Network (CTAN). The host-names are: ftp.dante.de, ftp.tex.ac.uk, ftp.shsu.edu; the CTAN directories are: /pub/tex/macros/latex209/contrib/elsevier, /pub/archive/macros/latex209/contrib/elsevier, /tex-archive/macros/latex209/contrib/elsevier, respectively. *No changes from the accepted version are permissible, without the explicit approval of the Editor. The Publisher reserves the right to decide whether to use the author's file or not.* If the file is sent by e-mail, the name of the journal should be mentioned in the "subject field" of the message to identify the paper. Authors should include an ASCII table (available from the Publisher) in their files to enable the detection of transmission errors.

Publication information:
Computer Methods in Applied Mechanics and Engineering (ISSN 0045-7825). For 1998 volumes 151–163 are scheduled for publication. Subscription prices are available upon request from the Publisher. Subscriptions are accepted on a prepaid basis only and are entered on a calendar year basis. Issues are sent by surface mail except to the following countries where Air delivery via SAL mail is ensured: Argentina, Australia, Brazil, Canada, Hong Kong, India, Israel, Japan, Malaysia, Mexico, New Zealand, Pakistan, PR China, Singapore, South Africa, South Korea, Taiwan, Thailand, USA. For all other countries airmail rates are available upon request. Claims for missing issues should be made within six months of our publication (mailing) date.

Orders, claims, and product enquiries
Please contact the Customer Support Department at the Regional Sales Office nearest you:

New York
Elsevier Science
P.O. Box 945
New York, NY 10159-0945
USA
Tel. (+1)212-633-3730
[Toll free number for North American customers: 1-888-4ES-INFO (437-4636)]
Fax (+1)212-633-3680
e-mail usinfo-f@elsevier.com

Amsterdam
Elsevier Science
P.O. Box 211
1000 AE Amsterdam
The Netherlands
Tel. (+31)20-4853757
Fax (+31)20-4853432
e-mail nlinfo-f@elsevier.nl

Tokyo
Elsevier Science
9-15 Higashi-Azabu 1-chome
Minato-ku, Tokyo 106
Japan
Tel. (+81)3-5561-5033
Fax (+81)3-5561-5047
e-mail info@elsevier.co.jp

Singapore
Elsevier Science
No. 1 Temasek Avenue
#17-01 Millenia Tower
Singapore 039192
Tel. (+65)434-3727
Fax (+65)337-2230
e-mail asiainfo@elsevier.com.sg

Advertising information
Advertising orders and enquiries may be sent to: **International:** Elsevier Science, Advertising Department, The Boulevard, Langford Lane, Kidlington, Oxford OX5 1GB, UK, Tel. (+44)(0)1865 843565, Fax (+44)(0)1865 843976. **USA and Canada:** Weston Media Associates, Daniel Lipner, P.O. Box 1110, Greens Farms, CT 06436–1110, USA, Tel. (+1)(203)261-2500, Fax (+1)(203)261-0101. **Japan:** Elsevier Science Japan, Marketing Services, 1-9-15 Higashi-Azabu, Minato-ku, Tokyo 106, Japan, Tel. (+81)3-5561-5033; Fax (+81)3-5561-5047.